AIP | Physics of Plasmas

Full toroidal plasma response to externally applied nonaxisymmetric magnetic fields

Yueqiang Liu, A. Kirk, and E. Nardon

Citation: Phys. Plasmas **17**, 122502 (2010); doi: 10.1063/1.3526677
View online: http://dx.doi.org/10.1063/1.3526677
View Table of Contents: http://pop.aip.org/resource/1/PHPAEN/v17/i12
Published by the American Institute of Physics.

Related Articles

Collision frequency dependence of polarization current in neoclassical tearing modes
Phys. Plasmas 19, 032120 (2012)

Effects of beam temperature and density variation on the growth rate of a two-stream free electron laser
Phys. Plasmas 19, 032114 (2012)

The limits and challenges of error field correction for ITER
Phys. Plasmas 19, 056111 (2012)

Dynamic contraction of the positive column of a self-sustained glow discharge in molecular gas
Phys. Plasmas 19, 033512 (2012)

Wall-locking of kink modes in a line-tied screw pinch with a rotating wall
Phys. Plasmas 19, 056104 (2012)

Additional information on Phys. Plasmas

Journal Homepage: http://pop.aip.org/
Journal Information: http://pop.aip.org/about/about_the_journal
Top downloads: http://pop.aip.org/features/most_downloaded
Information for Authors: http://pop.aip.org/authors

ADVERTISEMENT

Downloaded 04 Apr 2012 to 129.16.35.96. Redistribution subject to AIP license or copyright; see http://pop.aip.org/about/rights_and_permissions

Full toroidal plasma response to externally applied nonaxisymmetric magnetic fields

Yueqiang Liu,[1,a)] A. Kirk,[1] and E. Nardon[2]
[1]*Euratom/CCFE Fusion Association, Culham Science Centre, Abingdon OX14 3DB, United Kingdom*
[2]*Euratom/CEA Fusion Association, 13108 St. Paul-lez-Durance, France*

(Received 5 October 2010; accepted 22 November 2010; published online 9 December 2010)

The plasma response to resonant magnetic perturbation (RMP) and nonresonant perturbation fields is computed within a linear, full toroidal, single-fluid resistive magnetohydrodynamic framework. The response of resonant harmonics depends sensitively on the plasma resistivity and on the toroidal rotation. The response of nonresonant harmonics is not sensitive to most of the plasma parameters, except the equilibrium pressure. Both midplane and the off midplane odd parity RMP coils trigger a similar field response from the plasma. The RMP fields with different toroidal mode numbers trigger qualitatively similar plasma response. A simple model of the electron diamagnetic flow suggests significant effects both in the pedestal region and beyond. [doi:10.1063/1.3526677]

I. INTRODUCTION

It is now well established that the resonant magnetic perturbation (RMP) fields play a significant role in mitigation of the type I edge localized modes (ELMs) for H-mode tokamak plasmas.[1–3] At high enough plasma pressure, these fields can also trigger marginally stable magnetohydrodynamic (MHD) modes, leading to the so-called resonant field amplification (RFA) effect.[4,5] Both these phenomena involve interaction of the plasma with the external magnetic fields. Both cases can eventually lead to the formation of three-dimensional plasma equilibria in a tokamak, in which the stability properties, the momentum, and energy confinement may be significantly affected, compared to the axisymmetric equilibria. There are also differences between these two cases, such as the equilibrium plasma pressure, and the resistive (normally in the ELM mitigation case) versus the ideal (normally in the RFA case) plasma response.

This work focuses on understanding of the resistive plasma response to nonaxisymmetric fields produced by RMP coils at relatively low plasma pressures (below the no-wall beta limit for the ideal kink mode). We rely on a full MHD model, as opposed to the reduced MHD models.[6–10] Our modeling also assumes full toroidal geometry with realistic plasma shaping, improving on cylindrical approximations.[11,7,10] The full toroidal coupling allows us to study not only the response of the resonant harmonics to the RMP fields, but also that from the nonresonant harmonics. In this work, we try to understand the *linear* response of the plasma to the RMP fields, fixing the plasma rotation. Meanwhile, significant efforts have been devoted to investigating the *nonlinear* RMP penetration dynamics.[6,12,7,13,8–10] In particular, Refs. 12 and 13 involve a nonlinear study in a full geometry with the full MHD model. Numerical difficulties force these computations to be made at rather low Lundquist numbers. Our linear response computations can afford realistic plasma resistivity without numerical problems.

Although our model is primarily based on the single-fluid approximation, we do consider some two-fluid effects, in particular the diamagnetic flow of electrons. These effects have been shown important for the RMP field penetration.[14,11,9,10]

We propose a full toroidal equilibrium of the ELMy H-mode type, with the plasma boundary shape and all the equilibrium profiles analytically specified. This allows easier future benchmarking with other codes. Based on this equilibrium, we perform a systematic study of the RMP field induced plasma response by varying the plasma conditions (resistivity, rotation, pressure) and the RMP coil configuration (midplane coils, off midplane coils, various toroidal mode numbers) as well as by adding the electron diamagnetic flow into the model. The computations are carried out using the MHD code MARS-F.[15]

Section II describes the details of the model used for the RMP response computations. Section III specifies the plasma equilibrium and the RMP coils. Section IV reports the toroidal results. The conclusion and discussion are drawn in Sec. V.

II. FORMULATION

We compute the linear plasma response in the framework of single-fluid, resistive MHD approximation. The plasma model, with a *given* toroidal rotation $\mathbf{V}_0 = R\Omega\hat{\phi}$, is thus described by

$$i(\Omega_{\mathrm{RMP}} + n\Omega)\xi = \mathbf{v} + (\xi\cdot\nabla\Omega)R\hat{\phi}, \tag{1}$$

$$\begin{aligned} i\rho(\Omega_{\mathrm{RMP}} + n\Omega)\mathbf{v} &= -\nabla p + \mathbf{j}\times\mathbf{B} + \mathbf{J}\times\mathbf{b} - \rho[2\Omega\hat{\mathbf{Z}}\times\mathbf{v} + (\mathbf{v}\cdot\nabla\Omega)R\hat{\phi}] \\ &\quad - \rho\kappa_{\|}|k_{\|}v_{\mathrm{th},i}|[\mathbf{v} + (\xi\cdot\nabla)\mathbf{V}_0]_{\|}, \end{aligned} \tag{2}$$

$$\begin{aligned} i(\Omega_{\mathrm{RMP}} + n\Omega)\mathbf{b} &= \nabla\times(\mathbf{v}\times\mathbf{B}) + (\mathbf{b}\cdot\nabla\Omega)R\hat{\phi} - \nabla\times(\eta\mathbf{j}), \end{aligned} \tag{3}$$

$$i(\Omega_{\mathrm{RMP}} + n\Omega)p = -\mathbf{v}\cdot\nabla P - \Gamma P\nabla\cdot\mathbf{v}, \tag{4}$$

a)Electronic mail: yueqiang.liu@ccfe.ac.uk.

Downloaded 04 Apr 2012 to 129.16.35.96. Redistribution subject to AIP license or copyright; see http://pop.aip.org/about/rights_and_permissions

$$\mathbf{j} = \nabla \times \mathbf{b}, \tag{5}$$

where R is the plasma major radius, $\hat{\phi}$ the unit vector along the geometric toroidal angle ϕ of the torus, and $\hat{\mathbf{Z}}$ the unit vector in the vertical direction in the poloidal plane. Ω_{RMP} is the excitation frequency of the RMP field. n is the toroidal harmonic number. For a linear response of axisymmetric equilibria, we need to consider a single n only. The plasma resistivity is denoted by η. The variables $\xi, \mathbf{v}, \mathbf{b}, \mathbf{j}, p$ represent the plasma displacement, perturbed velocity, magnetic field, current, and pressure, respectively. The equilibrium plasma density, field, current, and pressure are denoted by ρ, $\mathbf{B}$, $\mathbf{J}$, and P, respectively.

The last term in Eq. (2) describes the effect of parallel sound wave damping,[16] where κ is a numerical coefficient determining the damping "strength." $k_{\parallel}=(n-m/q)/R$ is the parallel wave number, with m being the poloidal harmonic number and q the safety factor. $v_{\mathrm{th},i}=\sqrt{2T_i/M_i}$ is the thermal ion velocity, with T_i, M_i being the thermal ion temperature and mass, respectively. The parallel component of the perturbed velocity is taken along the equilibrium field line. In this work, we assume $\kappa_{\parallel}=1.5$, corresponding to a strong sound wave damping.

The RMP field is generated by the source current $\mathbf{j}_{\mathrm{RMP}}$ flowing in the RMP coils,

$$\nabla \times \mathbf{b} = \mathbf{j}_{\mathrm{RMP}}, \quad \nabla \cdot \mathbf{j}_{\mathrm{RMP}} = 0. \tag{6}$$

In MARS-F, the source current is specified as a surface current at the radial location of the RMP coils. The toroidal component of $\mathbf{j}_{\mathrm{RMP}}$ has a finite but narrow width along the poloidal angle, mimicking the point-wise RMP coil current on the poloidal plane. The current density $\mathbf{j}_{\mathrm{RMP}}$ varies as $\exp(in\phi)$ along the toroidal angle ϕ. The poloidal component of $\mathbf{j}_{\mathrm{RMP}}$ is obtained by the divergence-free condition.

The resistive wall is modeled as a thin shell, satisfying a jump condition for the tangential field due to the induced eddy current in the wall. The thin wall jump condition, the plasma equations (1)–(5), and the RMP coil equation (6) are solved together with the vacuum equation outside the plasma,

$$\nabla \times \mathbf{b} = 0, \quad \nabla \cdot \mathbf{b} = 0. \tag{7}$$

Note that for RMP response modeling, we also make use of the divergence-free condition for the total field perturbation $\mathbf{b}$ in the plasma region by replacing one of the equations in the Ohm's law (3) by $\nabla \cdot \mathbf{b}=0$. The plasma-vacuum interface conditions are the continuity of the normal component of the field $\mathbf{b}$ and the (total) perturbed pressure balance condition. The former is satisfied automatically by solving for the total $\mathbf{b}$ field across all regions.

We briefly discuss the relevance of various MARS-F components to the RMP ELM suppression experiments.

A. Linearity of the response model

The linear response model involves only one aspect of the field penetration dynamics in the ELM suppression experiments, namely, how the plasma responds to the externally applied field. The other important aspect—how the external field affects the plasma equilibrium flow—is not considered. Nevertheless, the model presents a significant step forward, compared to the pure external field, in understanding the field line stochastization during the ELM suppression. In addition, linear response computations with artificial scaling of rotation frequency offer a "perturbative" approach in studying the rotation effect. The model can be more directly applicable to experimental situations, where the plasma flow is not significantly modified by RMP fields.

B. Geometry

The full toroidal geometry and the realistic plasma shape are used in the MARS-F model. This is important to gain a quantitative interpretation of experiments. The plasma shaping effect can be of particular significance for the plasma edge response. One example is shown in a recent investigation,[17] where we use MARS-F to model the RMP response of MAST plasmas,[3] and find that the plasma displacement near the X-points plays an important role for the experimentally observed density pump-out effect.

C. Resistive-inertial model

MARS-F formulation describes the resistive and inertial response of the plasma. The so-called resistive-inertial model is valid if the Lundquist number S and the plasma rotation frequency Ω normalized by the Alfvén frequency satisfy a condition $Q \equiv S^{1/3}\Omega \lesssim 1$, and the ratio P of the resistive diffusion time to the plasma viscous diffusion time satisfies $P \lesssim Q^{3/2}$.[18] The first condition for the validity of the resistive-inertial layer model is normally satisfied in the tokamak plasma edge region, where the electron temperature is low ($S \sim 10^4 - 10^6$) and the plasma rotation is slow ($\Omega < 10^{-2}$). The second condition can be satisfied for edge plasmas with low temperature and relatively high density, such that $P < 1$. (This condition is always satisfied in the MARS-F model, since we assume a vanishing plasma viscosity.) The plasma core region, with the S value of order 10^8 and the Ω value of order 10^{-2}, is better described by the so-called inertial layer model.[18]

D. Sound wave damping model

At low plasma pressure, this damping term has a minor effect on the plasma response. It becomes important only when the plasma pressure approaches or exceeds the no-wall beta limit.[19] For these high pressure plasmas, experimental results[4,5] seem to suggest an important role played by some strong damping mechanism(s) (either parallel sound wave damping, or kinetic damping, or some other possible damping mechanisms) on the plasma response.

Finally, we mention that MARS-F model has been used to study the RMP response of DIII-D plasmas,[20] the ELM mitigation experiments in MAST,[17] as well as the RMP response of ITER plasmas.[17]

Downloaded 04 Apr 2012 to 129.16.35.96. Redistribution subject to AIP license or copyright; see http://pop.aip.org/about/rights_and_permissions

III. TOROIDAL EQUILIBRIUM AND COILS CONFIGURATION

We consider a toroidal equilibrium, in which both the plasma boundary shape and the equilibrium current, density, pressure, and rotation profiles are specified by analytic formulas. The major radius is assumed to be $R_0=3$ m. The vacuum toroidal field at the plasma center is $B_0=1.5$ T. (We note that the choice of R_0 and B_0 values is somewhat arbitrary. Since they enter into the MHD equations only as scaling parameters, their values do not change the eventual physics conclusions.) The plasma boundary (R_p,Z_p) has an aspect ratio of $R_0/a=3$, an elongation factor of $\kappa=1.6$, and the triangularity $\delta=0.3$,

$$R_p = R_0 + a\cos(\theta + \delta\sin\theta),$$

$$Z_p = \kappa a \sin\theta.$$

This plasma boundary shape is typical for some of the JET plasmas. A conformal wall is assumed at the minor radius $r_w=1.3a$. For static RMP response, however, the wall does not play a role.

The surface averaged toroidal plasma current density is specified as

$$\langle J_\phi\rangle = J_0(1-s^2),$$

where $J_0=2$ is the central current density, normalized by $B_0/(\mu_0 R_0)$. μ_0 is the vacuum magnetic permeability. $s\equiv\sqrt{\psi_p}$, ψ_p is the normalized poloidal flux, with $\psi_p=0$ at the plasma center, and $\psi_p=1$ at the plasma boundary.

In order to introduce a pedestal in the plasma edge region, we define a function

$$f(s) \equiv \frac{(s-s_0)^2}{(1-s_0)^2}H(s-s_0),$$

where $s_0=0.95$, $H(x<0)=0$, $H(x>0)=1$. The plasma density profile (normalized to unity at the plasma center) is then specified as

$$N(s) = 1-(1-N_0)(1-f)\frac{s^2}{s_0^2},$$

with $N_0=0.5$. The temperature profile (normalized to unity at the plasma center) for thermal ions and electrons is

$$T_i = T_e = (1-f)\left(1-s_1 s^2+\tfrac{1}{3}s^3\right),$$

with $s_1=1.2s_0$. Finally, the plasma rotation profile is defined as

$$\omega_{\rm rot} = (\omega_0-\omega_1)(1-2s^2+s^3)+\omega_1,$$

where ω_0 is the rotation frequency at the plasma center $s=0$. ω_1 specifies the plasma edge $(s=1)$ rotation frequency, normally a small number compared to ω_0.

The choice of the above analytic specifications of the equilibrium radial profiles is somewhat arbitrary. We only aim at reproducing certain qualitative features of a typical ELMy H-mode plasma, as shown by Fig. 1, where the radial profiles for the equilibrium density, temperature, pressure, and the safety factor q are plotted. The pressure amplitude, normalized by B_0^2/μ_0, is scaled to achieve $\beta_N=1.46$. The q value is chosen to have the total plasma current of 1.28 MA. This gives $q_0=1.25$, $q_{95}=4.21$, $q_a=5.24$. The q-profile is computed by solving the actual Grad–Shafranov equation in the toroidal geometry. For the $n=1$ RMP field, we will have four resonant harmonics $m=2,3,4,5$ inside the plasma. The plasma rotation profile, assumed to be for ion flow, will be shown in Fig. 25.

This equilibrium has features of the hybrid ELMy H-mode plasma: a flat q-profile at the plasma center with the minimum q value close to 1; density and pressure pedestals near the plasma edge. This equilibrium is very stable with respect to the external pressure-driven ideal kink modes: the no-wall β_N limit is 3.99 for the $n=1$ mode, 4.14 for $n=2$, and 4.13 for $n=3$.

We consider two alternative coil configurations for generating the external field. The external coils are located outside the wall minor radius, near the outboard midplane, and specified by $(R,Z)=(4.98,1)$ m and $(4.98,-1)$ m. The two sets of internal coils are located inside the wall, with one set above, and the other below the outboard midplane. Their coordinates are specified by $(R,Z)=(3.77,1.22),(4.07,0.7),(3.77,-1.22),(4.07,-0.7)$, respectively. The external coils configuration resembles those of the so-called C-coils in DIII-D and the error field correction coils in JET (also used for the ELM mitigation experiments in JET). The internal coils resemble the so-called I-coils in DIII-D. These coils are used to suppress ELMs in DIII-D. The coils geometry is shown in Fig. 2, together with the plasma boundary and the wall shapes. We assume a single-n variation of the RMP coil current $I_{\rm RMP}=I_0\exp(in\phi)$ along the toroidal angle ϕ, with the current amplitude I_0 in the unit of kAt. In this work, a dc RMP field is assumed, i.e., $\Omega_{\rm RMP}=0$.

All the results shown in Sec. IV assume a curve-linear coordinate system (s,χ,ϕ), where the radial coordinate $s\equiv\sqrt{\psi_p}$ labels the equilibrium flux surface. ϕ is the geometric toroidal angle. The poloidal angle χ is chosen such that the equilibrium field lines, when plotted in the χ-ϕ plane, are straight. The associated Jacobian J for this coordinate system is $J\equiv 1/(\nabla s\cdot\nabla\chi\times\nabla\phi)=qR^2/F$, where q is the safety factor, R the major radius of the torus, and F the equilibrium poloidal current flux function. Both q and F are functions of the poloidal flux ψ_p only.

IV. RESULTS

A. Reference case

Since the aim of this work is to investigate the variation of various plasmas and coil parameters on the RMP response, we specify a reference case for later comparison. We consider an equilibrium with $\beta_N=1.46$, and with the $n=1$ RMP field for the external midplane coils. The plasma resistivity is uniform across the minor radius, with the corresponding Lundquist number $S\equiv\tau_R/\tau_A=1/\eta=10^5$, where τ_R is the resistive diffusion time of the plasma, τ_A is the Alfvén time, and η is the normalized resistivity. Note that this low value of Lundquist number is only realistic near the plasma edge, where the electron temperature is relatively low. In the hot plasma core region, it is expected that the S value can be

Downloaded 04 Apr 2012 to 129.16.35.96. Redistribution subject to AIP license or copyright; see http://pop.aip.org/about/rights_and_permissions

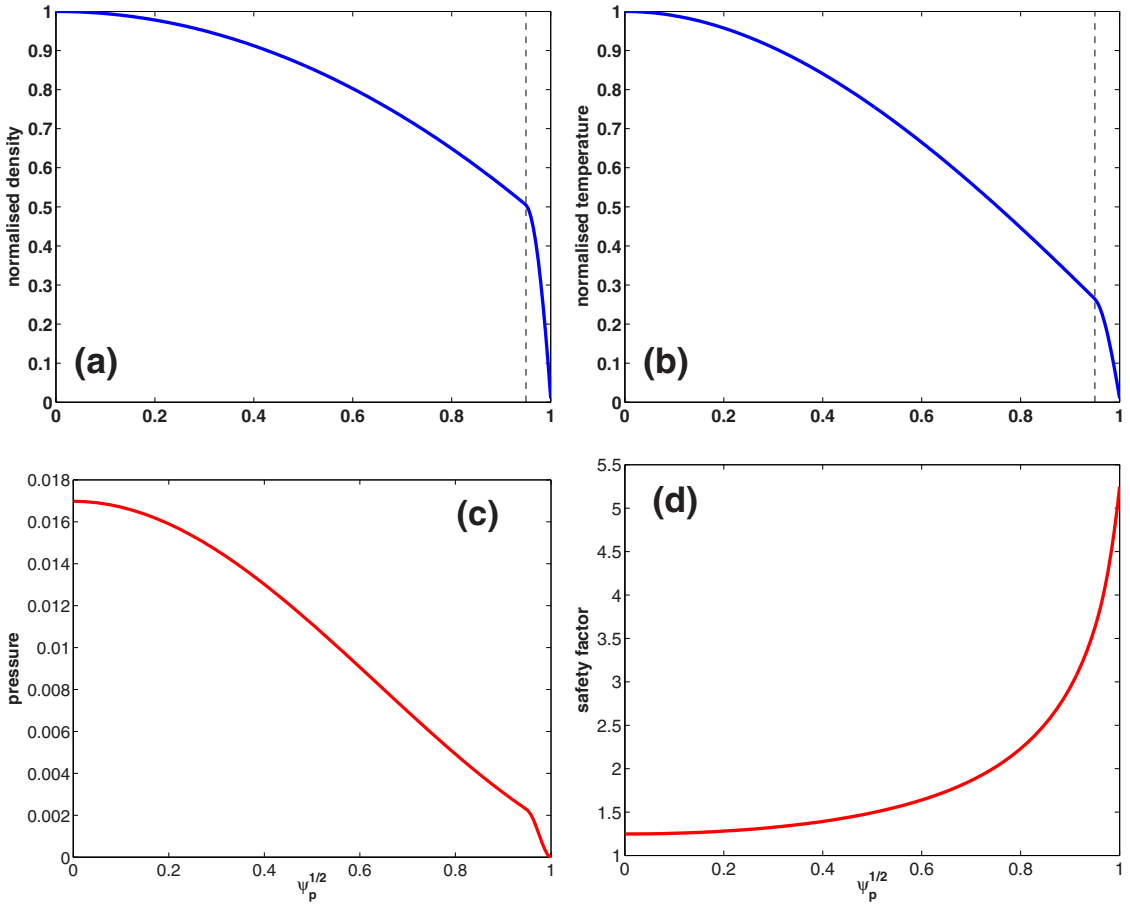

FIG. 1. (Color online) The equilibrium profiles for the plasma density, temperature, pressure, and the safety factor.

several orders of magnitude higher in present tokamaks. The effect of the plasma resistivity on the RMP response will be studied in Subsection IV B. We point out that the (uniform) resistivity profile is generally not consistent with the temperature profile. For the reference case, the plasma central rotation speed is assumed to be 3% of the Alfvén speed.

Figures 3(a) and 3(b) compare the spectrum of the radial component b^1 (in G/kAt of the RMP coil current) of the *total* and the *external* RMP field inside the plasma. Hereinafter, the total field refers to the sum of the external field (the free-space field of the RMP coils in the absence of the plasma and wall) and the pure response field due to the plasma and wall. Both fields have the same $n \neq 0$ toroidal mode number. The b^1 component is defined as

$$b^1 \equiv \frac{J}{R_0^2}\mathbf{b}\cdot\nabla s = \frac{J_s}{R_0^2}b_n,$$

where $J_s = J|\nabla s|$ is the surface Jacobian, and b_n is the normal component of the perturbed magnetic field. The b^1 component is essentially the perturbed flux function, and its poloidal harmonics are more meaningful in determining the corresponding magnetic islands width than those of the true normal component b_n. Figure 3 plots the amplitude of the poloidal harmonics of b^1 as a function of the harmonic number m, and along the minor radius ψ_p. Those harmonics with negative m numbers are all nonresonant harmonics. The location of the resonant surfaces, for which $q=m/n$, is marked by the + symbols.

The comparison of the RMP field spectra shows that the

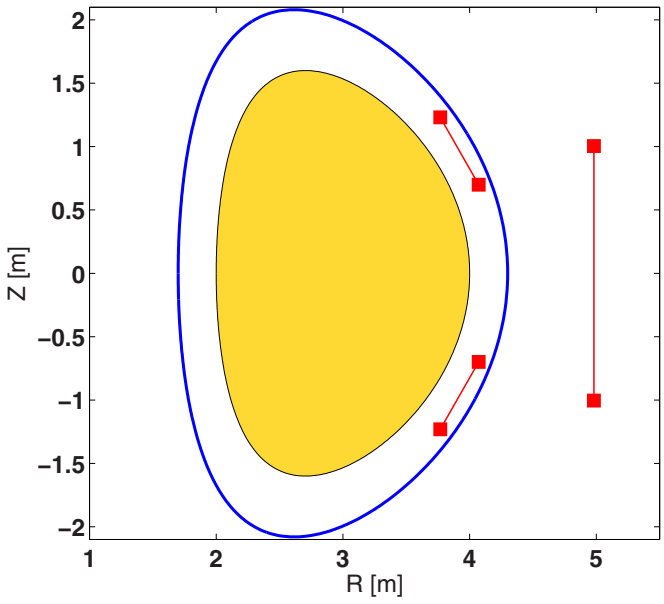

FIG. 2. (Color online) The plasma boundary, the wall shapes, and two alternatives of the RMP coils used in the simulation.

Downloaded 04 Apr 2012 to 129.16.35.96. Redistribution subject to AIP license or copyright; see http://pop.aip.org/about/rights_and_permissions

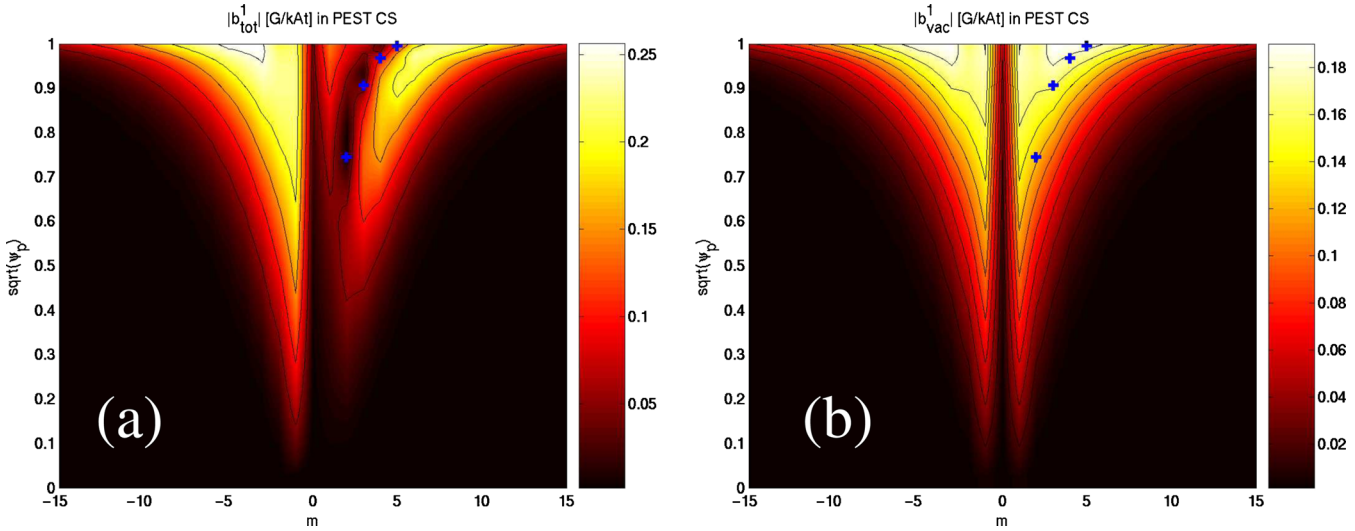

FIG. 3. (Color online) The amplitude of poloidal Fourier harmonics for (a) the total (external+plasma response) and (b) the external only, $n=1$ radial magnetic field b^1 in the whole plasma region. A straight-field-line flux coordinate system is used. ψ_p is the normalized poloidal flux. The external midplane coils with the $n=1$ current configuration are assumed. The location of resonant surfaces is marked by +.

major effect of the (resistive) plasma response, compared to the pure external field, is to reduce the field amplitude near the rational surfaces. As a result, the shape of the spectrum of the resonant part ($m>0$) is significantly modified by the plasma response. The most significant reduction of the resonant field harmonics occurs in the plasma core region, where the plasma response becomes more ideal either because of smaller resistivity, or thanks to faster plasma rotation. The latter case reflects the present modeling situation. [Theoretically, an ideal plasma response (either due to vanishing plasma resistivity or infinite plasma rotation) results in zero total field at resonant surfaces.] Meanwhile, the shape of the spectrum for the nonresonant part ($m<0$) remains almost unchanged, with only a moderate amplification (about 35% in this case) of the field amplitude. As will be shown later, this amplification depends strongly on the plasma pressure, and is due to the well known resonant field amplification phenomenon. The RFA effect of the plasma response is normally associated with the presence of marginally stable MHD modes in the plasma, such as the resistive wall mode (RWM) (Ref. 19) or the low-n peeling mode.[21] This resonance is due to the response of a mode (e.g., with the toroidal mode number of $n=1$) as a whole, having all (both resonant and nonresonant) poloidal harmonics.

Figures 4(a) and 4(b) offer a more detailed comparison of the b^1 field spectra near the plasma edge, between the total field and the external field. The amplitude of the $m=4,5$ resonant harmonics is clearly reduced at the location of the corresponding rational surfaces. The reduction is 51% for the $m=4$ harmonic and 57% harmonic for $m=5$. The amplitude, however, remains finite due to the resistive plasma response.

Figure 5 compares the radial profiles for the amplitude

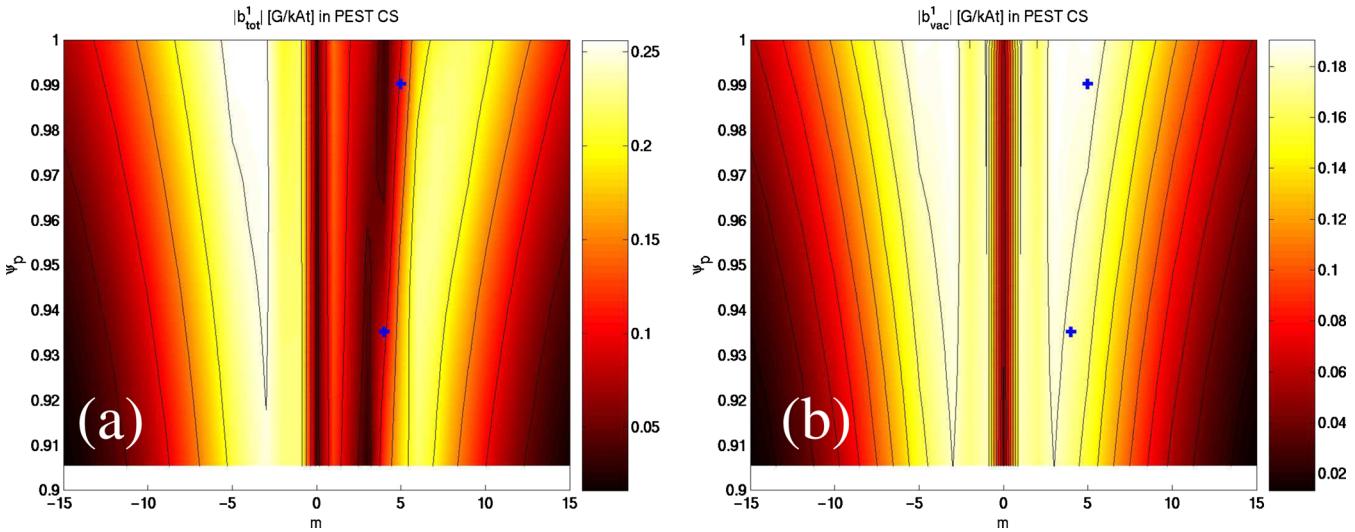

FIG. 4. (Color online) The amplitude of poloidal Fourier harmonics for (a) the total (external+plasma response) and (b) the external only, $n=1$ radial magnetic field b^1 in the plasma edge region. The external midplane coils with the $n=1$ current configuration are assumed. The location of resonant surfaces is marked by +.

Downloaded 04 Apr 2012 to 129.16.35.96. Redistribution subject to AIP license or copyright; see http://pop.aip.org/about/rights_and_permissions

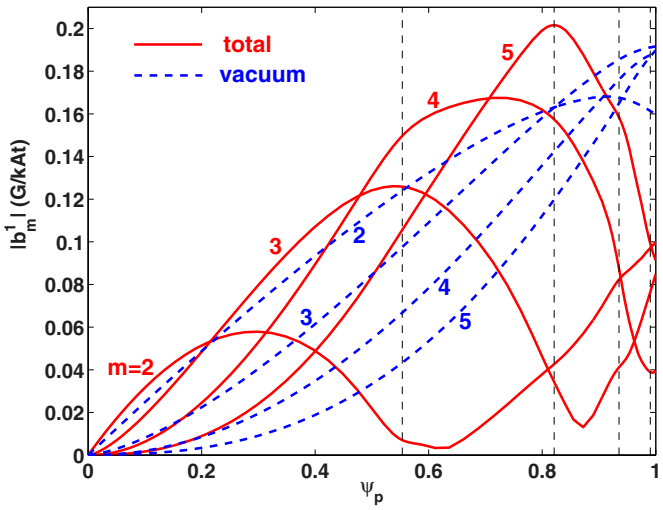

FIG. 5. (Color online) Comparison of radial profiles between the $n=1$ external radial field (dashed lines) produced by RMP coils and the total (external+plasma, solid lines) $n=1$ radial field for the resonant poloidal Fourier harmonics $m=2,3,4,5$. The dashed vertical lines indicate the radial locations of the corresponding rational surfaces with $q=m/n=2,3,4,5$.

of the poloidal Fourier harmonics $|b_m^1(\psi_p)|$ for all resonant harmonics $m=2,3,4,5$. As expected, the plasma response modifies substantially the shape of the radial profiles. As a result, even though the peak value of the radial profiles for each harmonic does not change dramatically, the local value at each corresponding rational surface changes a lot. Compared to the vacuum values of 0.124, 0.163, 0.176, and 0.187 G/kAt, the field amplitude is reduced to 5.8%, 21%, 51%, and 57% for the $m=2$, 3, 4, and 5 harmonics, respectively.

Another way to identify the plasma response is to plot the poloidal structure of normal field b_n along the plasma surface. Figure 6(a) compares the real part of b_n as a function of the geometric poloidal angle θ (θ generally differs from the poloidal angle χ for the straight-field-line coordinate system) at the plasma surface. The toroidal plane is chosen such that the RMP coil current I_{RMP} is wholly real. (For our reference case, the imaginary part of b_n, caused by the plasma response, is relatively small compared to the real part.) We notice that the total response field generally follows the shape of the external field. Considerable modification due to the plasma response occurs near the top/bottom of the torus, where $1 \lesssim |\theta| \lesssim 2$. The amplitude of the pure plasma response field for the reference case is shown by the solid line in Fig. 6(b). Generally, for an up-down symmetric equilibrium, with an up-down symmetric RMP coil geometry, one would expect an up-down symmetric plasma response field. The asymmetry shown in Fig. 6(b) is caused by the toroidal plasma rotation. Indeed, assuming an opposite rotation direction, the computed plasma response peaks in a reflective symmetry fashion, as shown by the dashed line in Fig. 6(b).

B. Effect of plasma resistivity

We first study the difference in the plasma response between ideal (i.e., with vanishing plasma resistivity) and resistive plasmas. Figure 7 shows a case of the ideal plasma response that differs from the reference case only by the plasma resistivity. As expected, the resonant harmonics of the total response field vanish at the corresponding rational surfaces. This is the major difference in the radial profiles, compared to those of the resistive plasma response shown in Fig. 5. As a consequence, the ideal plasma response excludes the possibility of formation of magnetic islands near the rational surfaces, while the resistive plasma response model, or the pure external field model, does allow the formation of islands.

We can also compare the peak values (over the plasma minor radius) of each poloidal harmonic $|b_m^1|$ of the radial field between the ideal, resistive plasma response, as well as the external field alone. Figure 8 makes such a comparison for both resonant and nonresonant harmonics. The resistive case ($\eta=1/S=10^{-5}$) is the reference case studied in Subsection IV A. The peak amplitude of the nonresonant harmonics is increased by the plasma RFA effect, while the peak amplitude of the resonant harmonics is generally reduced by the

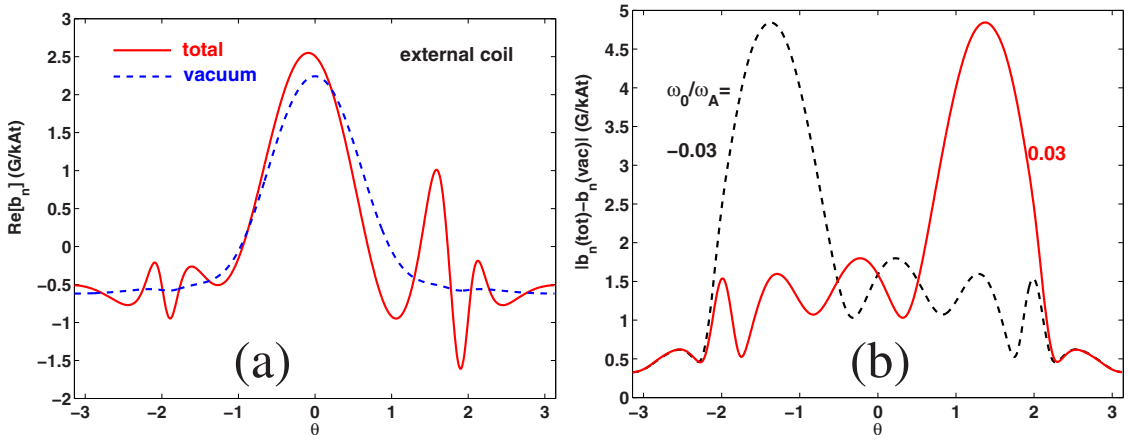

FIG. 6. (Color online) (a) Comparison of the normal component of the $n=1$ magnetic fields along the plasma boundary surface between the external field and the total (external+plasma) field. The amplitude of the $n=1$ plasma response field (total-external) is shown by the solid line in figure (b), which also shows the plasma response when the toroidal rotation switches direction. θ is the geometrical poloidal angle, with the origin defined at the magnetic axis, and $\theta=0$ corresponding to outboard midplane of the torus.

Downloaded 04 Apr 2012 to 129.16.35.96. Redistribution subject to AIP license or copyright; see http://pop.aip.org/about/rights_and_permissions

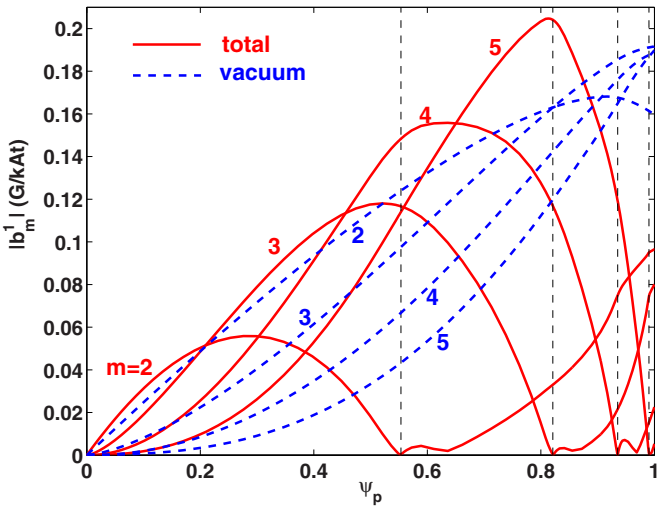

FIG. 7. (Color online) Comparison of radial profiles between the $n=1$ external radial field (dashed lines) produced by RMP coils and the total (external+plasma, solid lines) $n=1$ radial field for the resonant poloidal Fourier harmonics $m=2,3,4,5$. The plasma is assumed ideal. The dashed vertical lines indicate the radial locations of the corresponding rational surfaces with $q=m/n=2,3,4,5$. ψ_p is the normalized poloidal equilibrium magnetic flux.

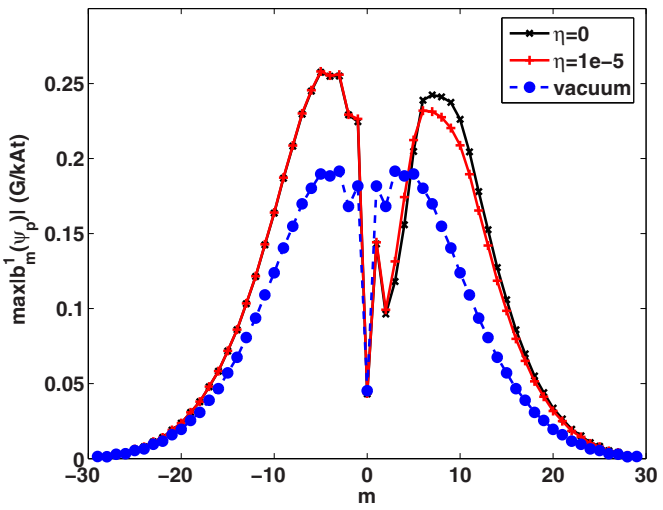

FIG. 8. (Color online) The maximal amplitude (along the minor radius) of the poloidal Fourier harmonics of the $n=1$ radial magnetic field b^1. The external field spectrum (dashed line and full "o") is compared with the total (external+plasma response) field spectrum (solid lines), assuming an ideal ("x") and a resistive (+) plasma. The resonant harmonics are $m=2,3,4,5$, and the remaining harmonics are nonresonant.

plasma response, compared to the external field. Both ideal and resistive plasma responses result in similar peak amplitude for all poloidal harmonics.

It is interesting to investigate the scaling law of the response of the resonant harmonics with the plasma resistivity. Figures 9(a) and 9(b) show radial profiles of the resonant harmonics $m=4,5$, respectively, with varying plasma resistivity η from 0 to 10^{-4}. At the rational surface, the total response field increases with increasing η, but the amplitude is generally below the vacuum level. We also notice that the linear response model predicts possible field amplification outside and further away from the rational surface radial location, even for resonant harmonics.

Figure 10 plots the dependence of the total response field amplitude at rational surfaces versus the plasma resistivity for resonant harmonics $m=2,3,4,5$. The solid lines with symbols represent the MARS-F results. The dashed lines are the analytic scaling law of $\eta^{3/4}$. According to a cylindrical model developed by Fitzpatrick,[18] the total response radial field is calculated as

$$\frac{b_r^{\mathrm{tot}}}{b_r^{\mathrm{vac}}} = \frac{2m}{-\Delta'_m + \Delta(\eta,\Omega)}, \tag{8}$$

where Δ'_m is the conventional tearing index. For the resistive-inertial plasma regime, the model predicts

$$\Delta(\eta,\Omega) = -2.124 e^{-i3\pi/8} S^{3/4} \left(\frac{\Omega}{\omega_A}\right)^{5/4}. \tag{9}$$

At a fixed rotation frequency Ω, and sufficiently large Lundquist number S (i.e., small enough resistivity η), we expect $|\Delta| \gg |\Delta'_m|$, and hence a scaling law of $\eta^{3/4}$ for the total radial field b_r^{tot}. This scaling is recovered by the MARS-F toroidal computations at the low resistivity limit.

At the very high resistivity limit $\eta \to \infty$, it is easy to see that the MHD equation (3) recovers the vacuum solution for the magnetic field. This limit is also correctly predicted by the MARS-F computation. Figure 10 shows that the total response field amplitude converges to the external field, as shown in Fig. 5, at very large η values.

C. Effect of toroidal plasma flow

In order to study the screening effect of the plasma flow on the RMP field, we vary the frequency of toroidal rotation, starting from the reference configuration. The radial profile of the rotation is kept fixed. As an example, Fig. 11(a) shows the $m=4$ resonant harmonic while decreasing the toroidal rotation frequency from $4\%\omega_A$ to $1\%\omega_A$ at the plasma center. The total response field is globally increased by reducing rotation. At the resistivity considered here ($S=10^5$), a rather strong response is computed at sufficiently slow rotation, near $1\%\omega_A$, indicating a strong scaling of the RMP response versus rotation. We also notice that at sufficiently slow rotation, the total response field amplitude can exceed the external field at the rational surface, yielding an amplification of the (linear) magnetic island, compared to the vacuum island. Therefore, without significant rotational screening effect, it is possible that the resistive plasma response enhances the magnetic island overlapping. We note that the relative rate between the increase of the field response and the decrease of rotation speed depends on the plasma resistivity. This rate becomes smaller at larger Lundquist number, as is also evident from the analytic model (9).

Figure 11(b) compares the peak amplitude of all the poloidal harmonics with varying plasma rotation speed. The nonresonant harmonics, with $m<0$, are not sensitive at all to the variation of rotation (at least in the range considered

Downloaded 04 Apr 2012 to 129.16.35.96. Redistribution subject to AIP license or copyright; see http://pop.aip.org/about/rights_and_permissions

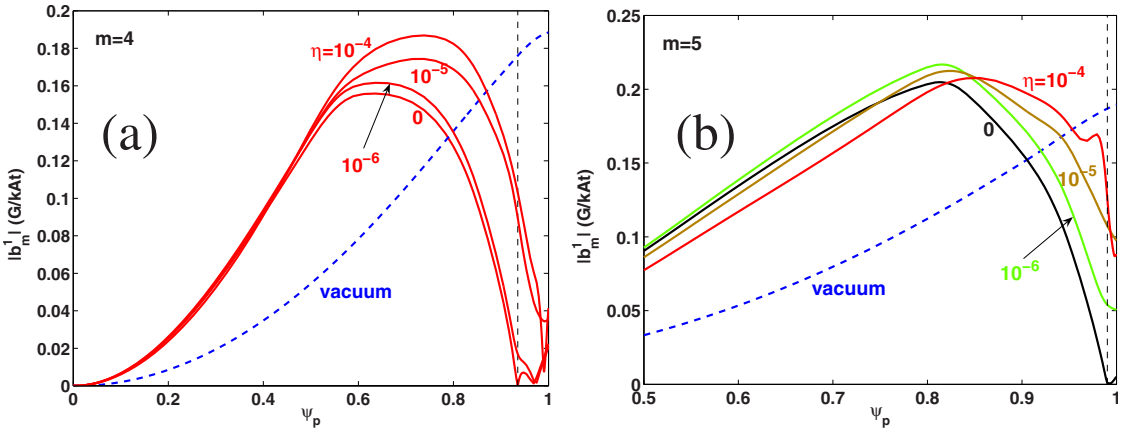

FIG. 9. (Color online) The radial profiles of the total (external+plasma response) radial field component with varying plasma resistivity for (a) the resonant harmonic $m/n=4/1$ and (b) the resonant harmonic $m/n=5/1$. Plotted are also the external field (dashed lines) components produced by RMP coils. The dashed vertical lines indicate the resonant surfaces $q=4$ and 5, respectively.

here), whereas the resonant harmonics, $m=2,3,4,5$, are very sensitive to rotation. Moreover, the nonresonant harmonics with positive m number, $m>5$, are also significantly amplified at slow rotation as a result of toroidal coupling of these harmonics to the resonant ones.

Figure 12 compares the MARS-F computed field response versus rotation, with the analytic scaling law (9) based on the resistive-inertial layer model. The $\omega_0^{-5/4}$ scaling is well recovered for fast enough rotation, especially for the low $m(m=2,3)$ harmonics. At slow rotation, the scaling law is not satisfied anymore, as also predicted by Eq. (8).

We summarize the results so far by showing contour plots of the resonant field amplitude versus the two most important plasma parameters in the resistive-inertial MHD model—the plasma rotation frequency and the plasma resistivity. Figures 13(a)–13(d) show such plots for all resonant harmonics $m=2,3,4,5$, respectively. In the region of fast rotation and small resistivity (right-bottom region in each figure), the scaling laws are well recovered, resulting in straight contour lines. In the region of slow rotation and large resistivity (top-left region), the plasma response is more complex: local maxima and minima in the amplitude are possible.

D. Effect of β

It is well known that the plasma RFA response, due to marginally stable MHD modes such as the resistive wall mode, is sensitive to the plasma pressure,[19,22] especially near the stability limits in β. In the ELM mitigation experiments with RMP coils, normally the plasma pressure is well below the no-wall beta limit for the ideal kink mode—this motivates our choice of $\beta_N=1.46$ for the reference case, which is far below the $(n=1)$ no-wall limit of 3.99. It is, however, certainly desirable to understand the plasma response to RMP coils with varying plasma pressure up to the no-wall beta limit. We notice that DIII-D experiments[23] also reported a heating power threshold, below which the ELM mitigation was not effective. The corresponding β_N limit was found to be about 1.4 for the plasmas considered in Ref. 23.

In this subsection, we vary the plasma pressure β_N, starting again from the reference case. Figure 14 shows the ratio of the peak amplitude of the total response field to that of the external field for four equilibria with increasing $\beta_N=0.49,1.46,2.51,3.57$. The last equilibrium approaches the no-wall limit. This ratio can be viewed as a global measure of RMP field amplification/reduction due to the plasma response. (But it does not reflect the local effect, in particular for the resonant poloidal harmonics.) The $m<0$ nonresonant harmonics are always amplified by the plasma, and the amplification is enhanced with increasing the plasma pressure. Since $q_a<6$ and $n=1$, the $m>5$ harmonics also have no resonant surfaces inside the plasma. These harmonics are generally amplified for the cases considered here, but there is no monotonic dependence of the amplification factor on β_N. This is primarily due to the strong coupling of these nonreso-

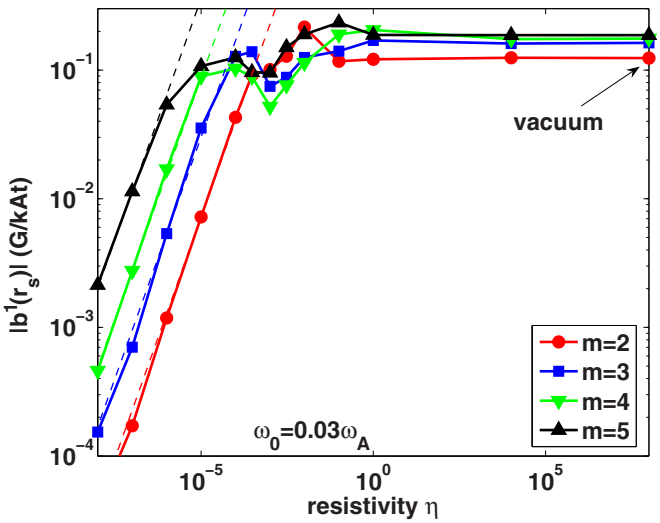

FIG. 10. (Color online) The MARS-F computed resistive plasma response to the $n=1$ RMP coils (the external midplane coils). The amplitude of the poloidal harmonics $m=2,3,4,5$ of the resonant (total, radial component) fields is computed at the corresponding rational surfaces and plotted against the normalized plasma resistivity $\eta\equiv S^{-1}$ at $\omega_0=3\times10^{-2}\omega_A$. The dashed lines correspond to the $\eta^{3/4}$ scaling. The $\eta\to\infty$ limit recovers the vacuum results.

Downloaded 04 Apr 2012 to 129.16.35.96. Redistribution subject to AIP license or copyright; see http://pop.aip.org/about/rights_and_permissions

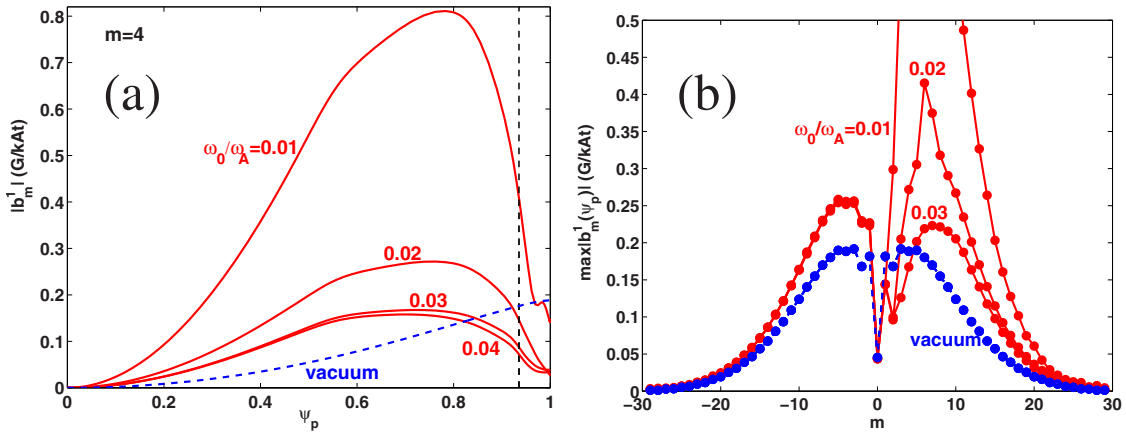

FIG. 11. (Color online) (a) The radial profiles of the resonant $m/n=4/1$ total (external+plasma response) radial field component with varying toroidal rotation frequency. The dashed vertical line indicates the $q=4$ resonant surface. (b) The maximal amplitude (along the minor radius) of all the poloidal Fourier harmonics of the $n=1$ total radial field. The resonant harmonics are $m=2,3,4,5$, and the remaining harmonics are nonresonant. Plotted are also the external field (dashed lines) components produced by RMP coils.

nant harmonics to the resonant ones, $m=2,3,4,5$. The resonant harmonics in this case are generally reduced by the plasma response.

We also notice a significant modification of the mode spectrum for the $\beta_N=3.57$ case: the $m=6$ nonresonant component becomes large. This is due to the fact that the plasma is close to the marginal stability for the ideal kink mode, hence a strong RWM response is triggered.[19,22] The poloidal structure of the pure plasma response also changes as β_N approaches the no-wall limit, as shown in Fig. 15.

Increasing pressure also results in a local increase of the total radial field for resonant harmonics. Figure 16 shows one example for the $m=4$ harmonic. The total field amplitude, at the resonant surface, increases with β_N.

E. Various coil geometry

Here we compare the plasma response to the external and internal RMP coils specified in Fig. 2. We first notice that with static RMP fields, the wall eddy current vanishes, and hence does not affect the plasma response. The relative position of the coils to the wall ("internal" or "external") does not have a physical significance. It is the radial position of the coils, their poloidal location/coverage, and the toroidal phasing of the coil currents that play roles in our model. We use the reference plasma with the $n=1$ coil current. Figure 17 shows the total field spectrum using the internal off midplane coils, assuming that the upper and the lower coil currents have the opposite sign (odd parity). The plasma is the same as for the reference case. Compared to the total field spectrum shown in Figs. 3(a) and 4, the internal coil configuration causes narrower spectrum band, especially near the plasma edge region. The peak amplitude of the radial field spectrum is more than a factor of 3 larger with the internal coils than that with the external midplane coils, with the same coil current and the same plasma condition. With assumed coil parity for the I-coils, this is primarily due to the proximity of the internal coils to the plasma surface. Compared to the external field, the plasma response has a similar effect as that for RMP field from the external coils, i.e., reducing the field amplitude near rational surfaces for resonant harmonics. Outside rational surfaces, however, we observe a much stronger field amplification due to the plasma response, compared to the external coil configuration. This is more clearly seen in Fig. 18(a).

Figures 18(a) and 18(b) compare the external RMP field with the total field including the plasma response for the internal coils. The plasma response causes both field reduction near rational surfaces and field amplification outside rational surfaces for resonant harmonics. The amplification effect is much stronger than the external coil case (Fig. 5). The amplification occurs mostly in the bulk plasma region, not in the edge region.

Figure 18(b) compares the normal field component along the plasma surface, between the external field and the total

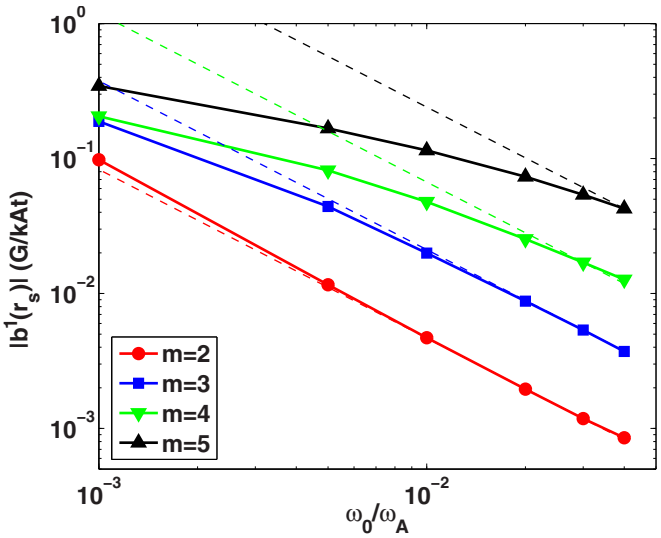

FIG. 12. (Color online) The MARS-F computed resistive plasma response to the $n=1$ RMP coils (the external midplane coils). The amplitude of the poloidal harmonics $m=2,3,4,5$ of the resonant (total, radial component) fields is computed at the corresponding rational surfaces and plotted versus the plasma rotation frequency at fixed resistivity $\eta=10^{-6}$. The dashed lines correspond to the $\omega_0^{-5/4}$ scaling.

Downloaded 04 Apr 2012 to 129.16.35.96. Redistribution subject to AIP license or copyright; see http://pop.aip.org/about/rights_and_permissions

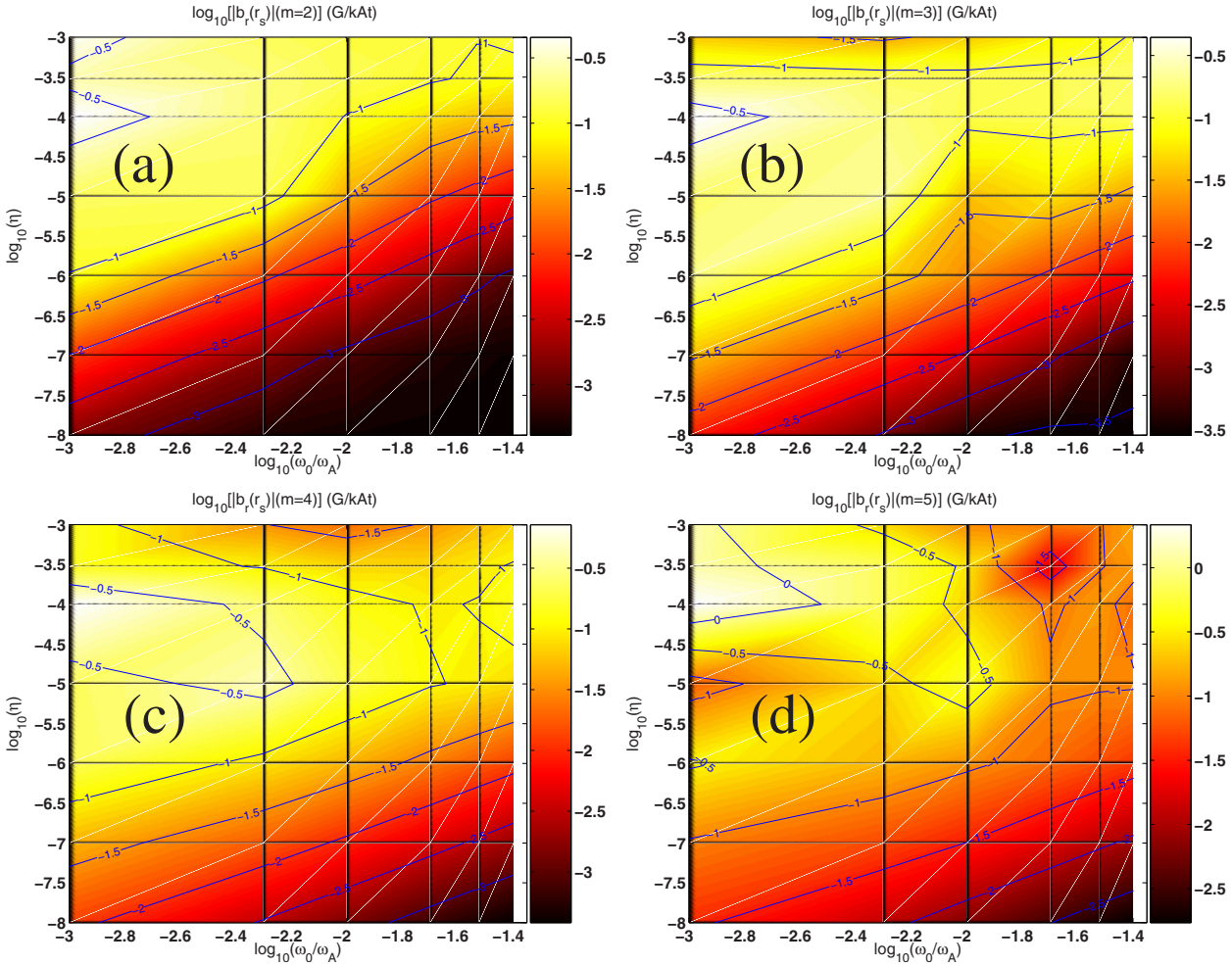

FIG. 13. (Color online) The local amplitude of the $n=1$ total (external+plasma response) radial field b^1 for the resonant harmonics (a) $m=2$, (b) $m=3$, (c) $m=4$, and (d) $m=5$. The field amplitude is computed at the corresponding rational surfaces. Both the plasma rotation speed ω_0 and the plasma resistivity η are varied.

field. Similar to the external coil case [Fig. 6(a)], internal coils also tend to cause a large response from the plasma, near the top/bottom region of the torus.

It is even more interesting to compare the pure plasma response field (i.e., the total field subtracted by the external field) caused by the external and internal coils. This is shown in Figs. 19(a) and 19(b). Here we also consider an even parity case for the internal coils, where both the upper and lower coil currents have the same sign. Despite a rather different spectrum of the excitation RMP field, the shape of the plasma response is similar between the odd parity internal coils and the external coils. The major difference is in the amplitude—the internal coils cause more than three times larger plasma response than the external coils with the same coil current. As already stated above, this factor of 3 is mainly caused by the proximity of the internal coils to the plasma surface. To confirm this, we moved the external coil to the same radial location of the internal coils without changing the fraction of the poloidal coverage. We obtained nearly the same amplitude for the pure plasma response field as that by the internal coils. Compared to the odd parity coils, the internal coils with even parity cause somewhat less response. More importantly, the radial shapes of the resonant harmonics are significantly different in the outer half of the plasma minor radius.

Figure 19(b) compares the poloidal distribution of the pure response field at the plasma edge for three cases. The odd parity internal coils and the external coils cause a similar shape of the response field, peaking near the bottom of the torus. The even parity external coils cause different poloidal distributions, peaking in a wide region of the low-field-side of the torus. Compared to the odd parity internal coils, the even parity coils trigger about 2.5 times smaller response field at the plasma edge, and the external coils trigger about three times smaller field.

The amplitude of the response field depends also somewhat on the poloidal coverage (i.e., the area) of the RMP coils. By reducing the coverage by 50% for the shifted external coils, we found that the amplitude of the plasma response field was reduced by about 40%—this is much less sensitive dependence than that of the radial location of the coils.

Downloaded 04 Apr 2012 to 129.16.35.96. Redistribution subject to AIP license or copyright; see http://pop.aip.org/about/rights_and_permissions

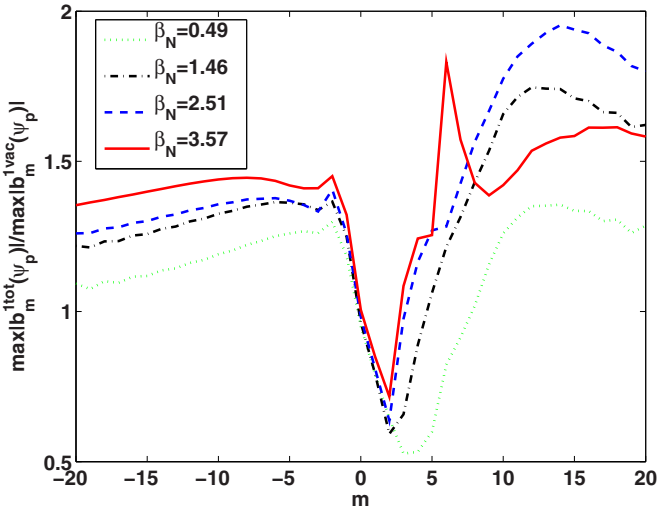

FIG. 14. (Color online) Ratio of the peak amplitude of total response field to that of the external field with varying plasma pressure (below the no-wall limit for the $n=1$ ideal kink mode). The peak amplitude is defined as the maximal amplitude over the plasma minor radius inside the plasma for each poloidal Fourier harmonics of the radial field b^1. The resonant harmonics are $m=2,3,4,5$.

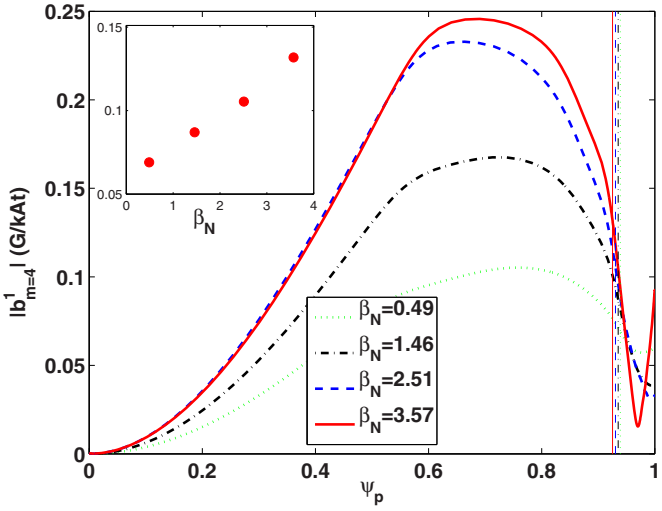

FIG. 16. (Color online) Amplitude of the $m=4$ resonant harmonic for the total (external+plasma response) radial field b^1 vs the plasma minor radius ψ_p, defined as the normalized equilibrium poloidal magnetic flux. The plasma pressure β_N is increased up to just below the no-wall limit for the $n=1$ ideal kink mode. The inserted subplot shows the field amplitude vs β_N at the $q=4$ rational surface, indicated by vertical dashed lines in the main plot. (The radial location of the rational surface slightly varies β_N.)

Different coil geometry yields different poloidal spectrum of the field perturbation. Figure 20 compares four configurations of the coil geometry. Plotted is the amplitude of poloidal harmonics of the external field alone (dashed lines) and the total response field (solid lines) computed at the plasma surface. Shifting the radial location of the midplane coils [(a) versus (b)] results mainly in the change of the amplitude, with minor modification to the field spectrum. Off midplane coils with odd parity (c) offer similar vacuum spectrum to that of midplane coils for $|m| \lesssim 10$. The field spectrum of off midplane even parity coils (d) is rather different. These similarities and differences may explain the observations from Fig. 19(b). Another significant feature, common for all coil configurations, is that the plasma response tends to reduce the amplitude of resonant harmonics (full circles), but amplifies the amplitude of nonresonant harmonics (open circles). The amplification is substantial for those nonresonant harmonics close to the resonant ones and with $m > nq_{\max}$.[24]

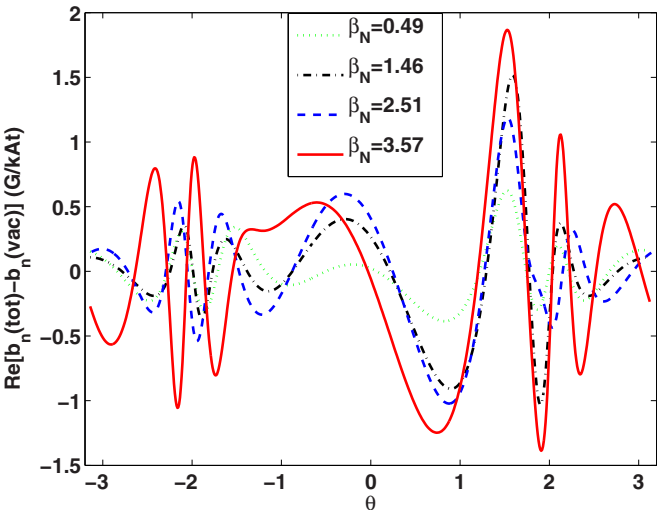

FIG. 15. (Color online) Real part of the normal component of the pure plasma response field plotted along the geometrical poloidal angle θ (with the magnetic axis as the origin). The normalized plasma pressure β_N is varied below the no-wall limit for the $n=1$ ideal kink mode.

The similarity of the pure plasma response, triggered by the midplane coils and the off midplane odd parity coils and shown by Fig. 19(b), is easy to understand in terms of the plasma field spectrum, as shown by Fig. 21. Indeed, these two types of coils cause a very similar plasma response field spectrum, in particular for all resonant and nonresonant harmonics with $|m| \lesssim 10$. On the other hand, the off midplane even parity coils trigger rather a different field spectrum for both resonant and nonresonant harmonics. For instance, for the resonant harmonic $m=5$, for which the difference seems to be the largest, both midplane coils and off midplane odd parity coils trigger a plasma response with nearly 90° toroidal phase shift, compared to the external field, while the off midplane even parity coils yield about 45° toroidal phase shift.

F. RMP response to $n>1$ fields

The ELM mitigation experiments often choose different toroidal number n as the dominant component for the RMP field. Normally, a lower n component yields a higher field amplitude with the same coil current. But a higher n component tends to create more resonant surfaces near the plasma edge region, which may be beneficial for the ELM suppression. Sometimes the low $n(n=1)$ configuration is not chosen to avoid causing large rotation damping in the plasma core by external fields. Here we study the plasma response to the RMP field with various n numbers. Figures 22(a) and 22(b) show the radial profiles of resonant poloidal harmonics for

Downloaded 04 Apr 2012 to 129.16.35.96. Redistribution subject to AIP license or copyright; see http://pop.aip.org/about/rights_and_permissions

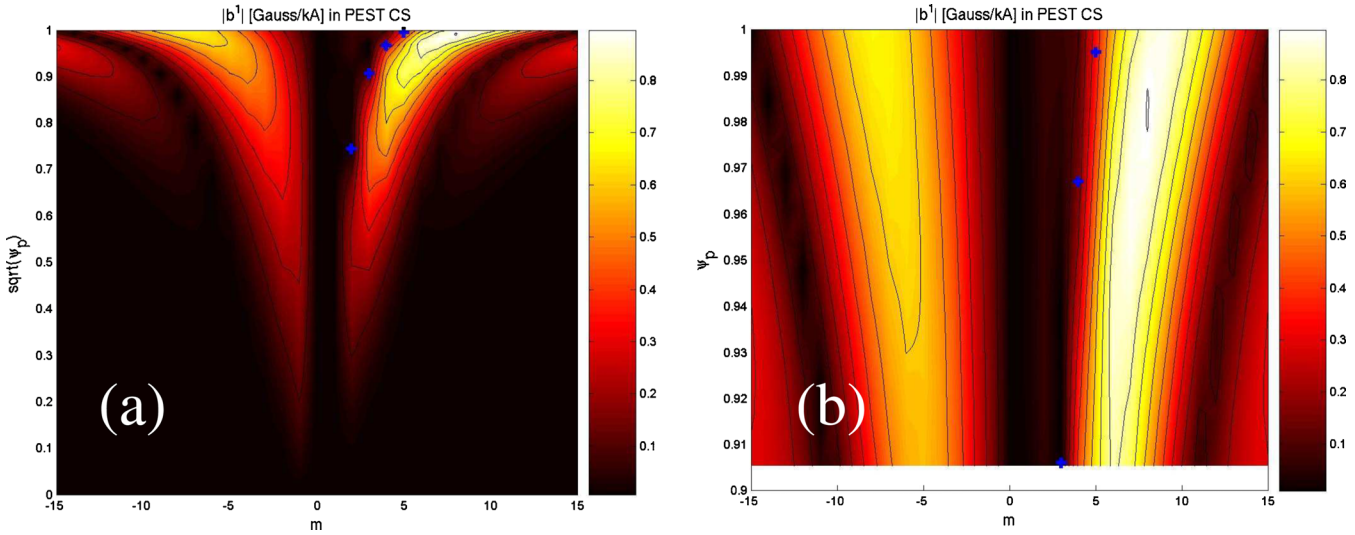

FIG. 17. (Color online) The amplitude of poloidal Fourier harmonics for the total (external+plasma response) $n=1$ radial magnetic field b^1 in (a) the whole plasma region and (b) the plasma edge region. The internal off midplane coils with odd parity are used.

the $n=2$ and 3 configurations, respectively. These configurations differ from the reference case (Fig. 5) only by the n number.

With increasing toroidal number n, more resonant harmonics are introduced into the plasma ($m=2-5$ for $n=1$, $m=3-10$ for $n=2$, and $m=5-15$ for $n=3$). The shape of the radial profiles for resonant harmonics also becomes more similar to that of the external field. In particular, no significant field amplification effect, outside rational surfaces, is observed for $n=2$ and 3, compared to the $n=1$ configuration. Meanwhile, the total field amplitude at rational surfaces, although reduced compared to the vacuum value, remains finite, thanks to the resistive plasma response.

The field amplitude at rational surfaces is better compared in Fig. 23, where we plot $b^1_m(q=m/n)$ at each rational surface $q=m/n$, versus the radial location $\psi_p(q=m/n)$ of the corresponding surface. Note that we show the amplitude only in the plasma edge region. Evidently, for each n, the total response field (solid lines) is significantly smaller than the external field (dashed lines). The reduction becomes larger toward the plasma core (note the difference in the slope of the curves between the external and the total field).

The global modification of the RMP field spectra by the plasma response is compared in Fig. 24 for $n=1,2,3$ configurations. The $m<0$ nonresonant harmonics are amplified for all m's and n's, but the amplification becomes weaker with higher n number. The peak amplitude of the resonant harmonics (denoted by full symbols) is generally reduced by the plasma response, with an exception for $m=5$, $n=1$. The $m>0$ nonresonant harmonics can be either amplified or reduced by the plasma response, depending on the m and n numbers. In general, the overall field spectrum is substantially changed, compared to that of the external field, for all $n=1,2,3$ coil configurations.

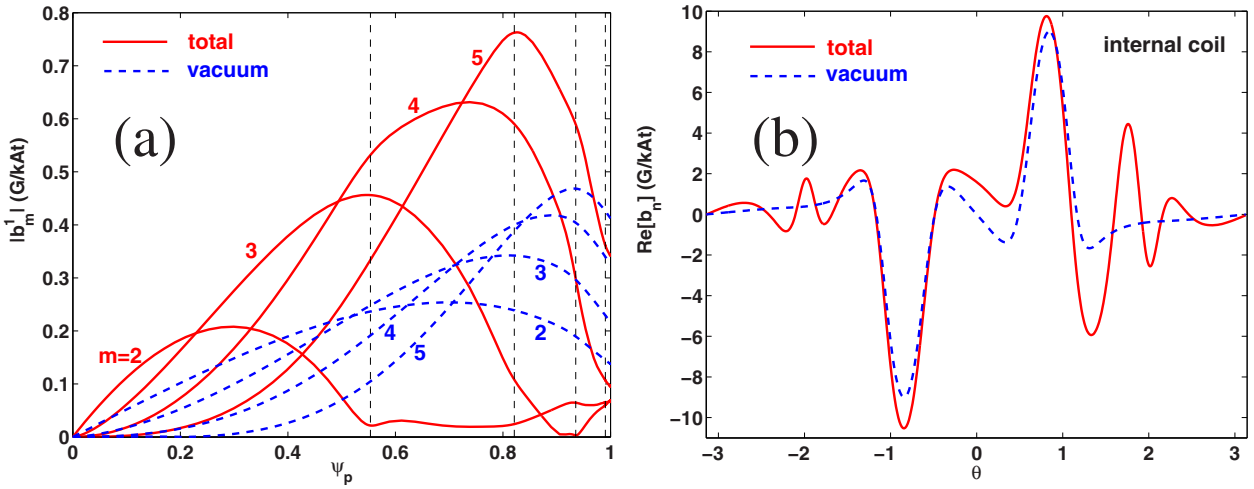

FIG. 18. (Color online) (a) Comparison of radial profiles between the $n=1$ external radial field (dashed lines) produced by the internal off midplane coils and the total (external+plasma, solid lines) $n=1$ radial field for the resonant poloidal Fourier harmonics $m=2,3,4,5$. The dashed vertical lines indicate the radial locations of the corresponding rational surfaces with $q=m/n=2,3,4,5$. (b) Comparison of the normal component of the $n=1$ magnetic fields along the plasma boundary surface between the external field and the total field. θ is the geometrical poloidal angle with the origin defined at the magnetic axis.

Downloaded 04 Apr 2012 to 129.16.35.96. Redistribution subject to AIP license or copyright; see http://pop.aip.org/about/rights_and_permissions

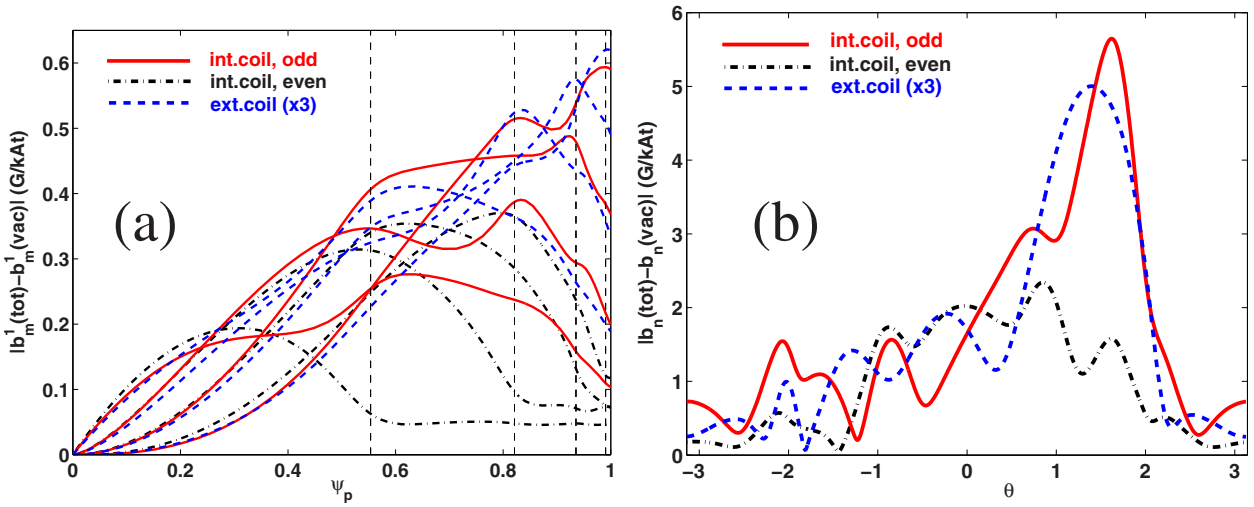

FIG. 19. (Color online) (a) Comparison of pure plasma response radial field profiles excited by the internal off midplane coils (solid lines for odd parity, dashed-dotted lines for even parity) and the external midplane coils (dashed lines). The resonant poloidal Fourier harmonics $m=2,3,4,5$ are shown. The dashed vertical lines indicate the radial locations of the corresponding rational surfaces with $q=m/n=2,3,4,5$. (b) Comparison of the amplitude of the pure plasma response field excited by the internal coils and the external coils vs the geometrical poloidal angle θ along the plasma surface. The amplitude of the plasma response to external coils is multiplied by a factor of 3 in the figures.

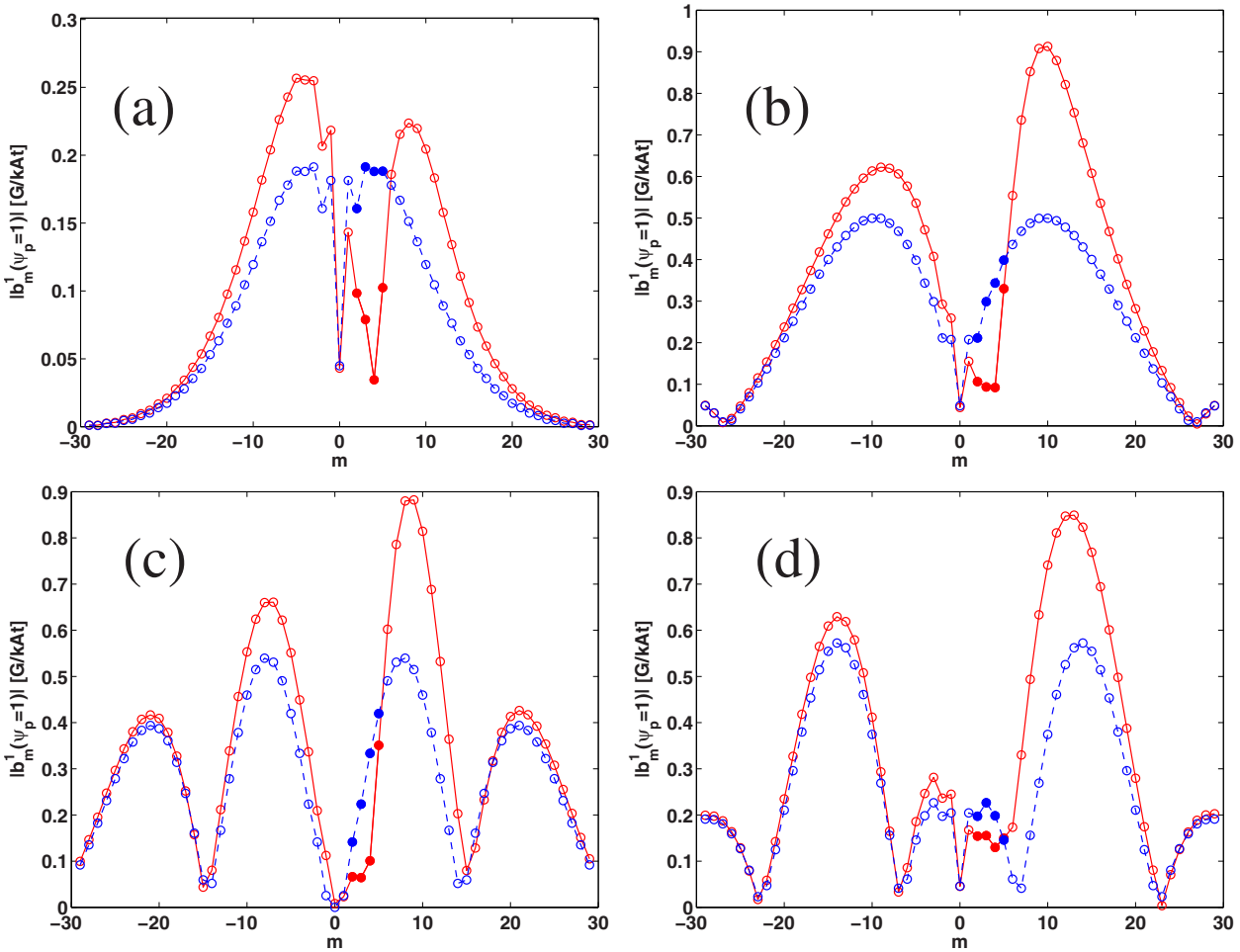

FIG. 20. (Color online) Comparison of the poloidal field spectrum (in PEST-like straight-field-line coordinate system) at the plasma surface between the external field (dashed) and the total response field (solid) for (a) external midplane coils, (b) internal midplane coils, (c) internal off midplane coils with odd parity, and (d) internal off midplane coils with even parity. The open (full) circles indicate nonresonant (resonant) harmonics.

Downloaded 04 Apr 2012 to 129.16.35.96. Redistribution subject to AIP license or copyright; see http://pop.aip.org/about/rights_and_permissions

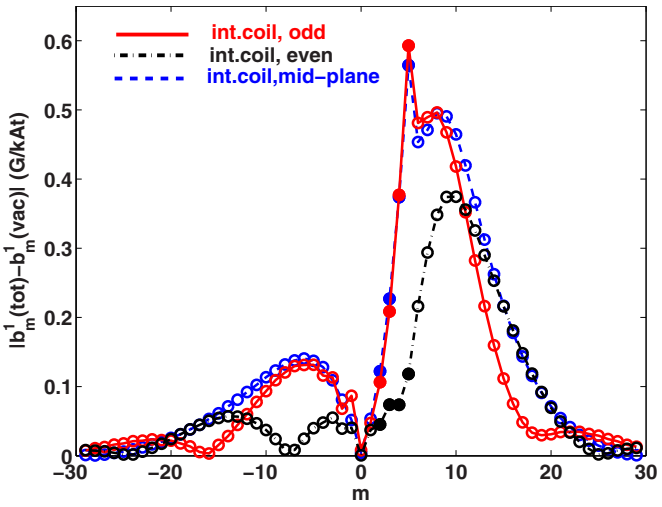

FIG. 21. (Color online) Comparison of the poloidal field spectrum (in PEST-like straight-field-line coordinate system) of the pure plasma response field at the plasma surface using internal off midplane coils with odd parity (solid) and even parity (dashed-dotted) as well as internal midplane coils (dashed). The open (full) circles indicate nonresonant (resonant) harmonics.

G. Effect of electron diamagnetic flow

In the ELMy H-mode plasma, with sharp variation of the electron density and temperature profiles in the pedestal region, the electron diamagnetic flow becomes large. And unlike ions, the electron diamagnetic flow normally does not cancel the $E\times B$ flow. As a result, the large electron flow near the plasma edge may have a significant screening effect on the RMP field penetration.[14,11,10] Here we try to pursue a qualitative understanding of the electron flow effect based on the MARS-F formulation. We make two fundamental assumptions. (i) We consider only the *toroidal projection* $\omega_E+\omega_{*,e}$ of the electron flow, which in reality is perpendicular to the equilibrium magnetic field line (i.e., having both toroidal and poloidal components). (ii) We assume that the major screening effect comes from the modification of Ohm's law due to the electron flow.[25] In other words, we shall replace the ion flow term $\Omega=\omega_E+\omega_{*,i}$ by $\Omega_e=\omega_E+\omega_{*,e}$ in Eq. (3) without changing any other terms. This allows us to study the electron flow effect, staying in the single-fluid approximation of MARS-F. Because of the assumptions stated above, the following results should be treated as qualitative.

Figure 25 compares the (toroidal) rotation profiles for ions and for electrons, respectively. The ion rotation Ω is assumed to be the plasma rotation and used in the reference configuration. The electron rotation frequency is computed as $\Omega_e=\Omega-\omega_{*,i}+\omega_{*,e}$, where, following Ref. 26, we define

$$\omega_{*,i}=-\frac{1}{e}\frac{T_i}{N}\frac{dN}{d\psi}\left(1+\frac{d\ln T_i}{d\ln N}\right), \tag{10}$$

$$\omega_{*,e}=\frac{1}{e}\frac{T_e}{N}\frac{dN}{d\psi}\left(1+1.71\frac{d\ln T_e}{d\ln N}\right), \tag{11}$$

where e is the electron charge and N the electron density. We notice that in the pedestal region, normally the electron density gradient is larger than the temperature gradient, and hence is the major contributor to the diamagnetic rotation.

The major differences between the ion flow and the electron flow shown in Fig. 25 are that (i) the electron flow changes direction near the plasma edge, resulting in a stationary point inside the plasma where the flow velocity vanishes; (ii) in the pedestal region, we have a substantial electron flow comparable with (even larger than) the core plasma flow. We point out that the cancellation between the ion-electron diamagnetic flow and the plasma fluid flow, although often occurring in tokamak experiments, may not always be the case—it obviously depends on the direction of the assumed (or measured) plasma flow with respect to the ion diamagnetic flow.

In the following, we start again with the reference case, only by replacing the ion flow by the electron flow in Ohm's law. Figures 26(a)–26(d) plot the external and the total response field for resonant harmonics $m=2,3,4,5$, respectively. We notice a sensitive dependence of the plasma re-

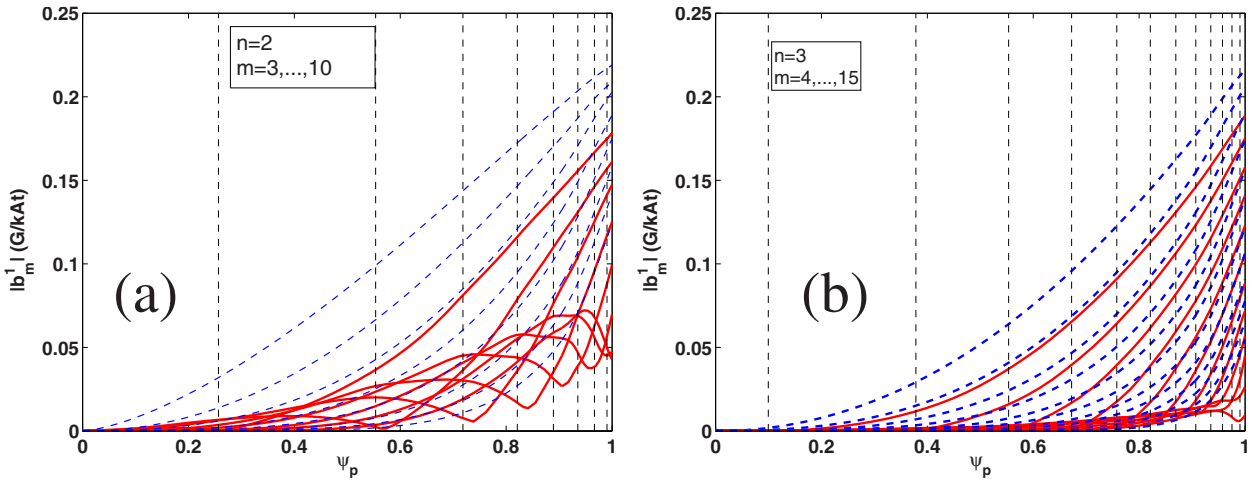

FIG. 22. (Color online) Comparison of radial profiles between the external radial field (dashed lines) produced by the external coils and the total (external +plasma, solid lines) radial field for the resonant Fourier harmonics with (a) $n=2$ and (b) $n=3$. The dashed vertical lines indicate the radial locations of the corresponding rational surfaces with $q=m/n$.

Downloaded 04 Apr 2012 to 129.16.35.96. Redistribution subject to AIP license or copyright; see http://pop.aip.org/about/rights_and_permissions

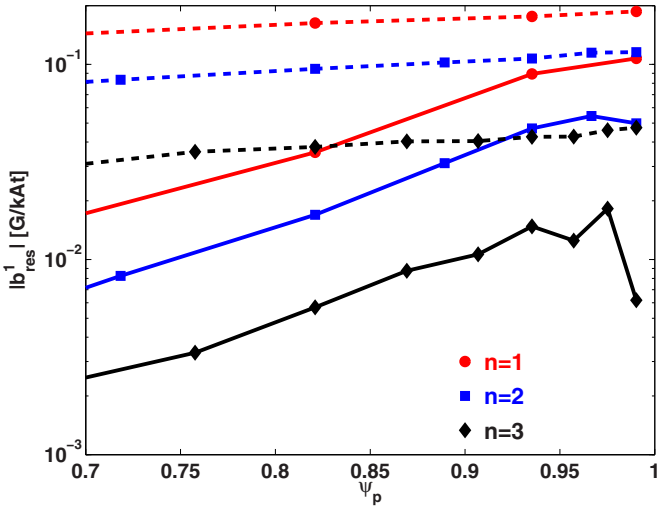

FIG. 23. (Color online) Amplitude of resonant harmonics of the radial field b^1 at corresponding rational surfaces for the $n=1,2,3$ RMP coil configurations. The total response field (solid lines) is compared with the external field (dashed lines).

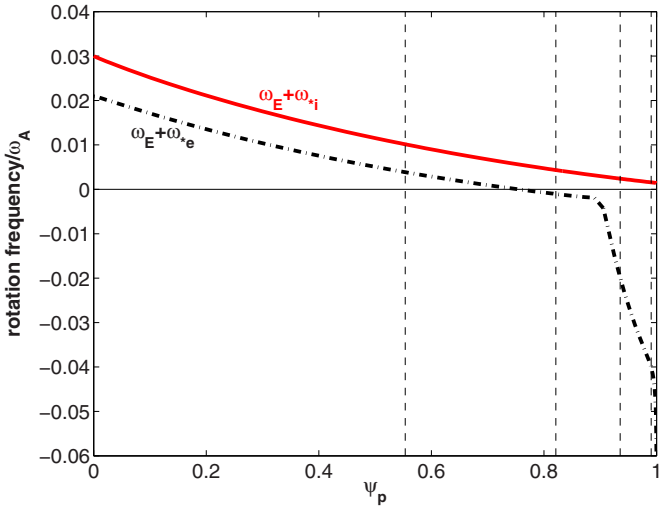

FIG. 25. (Color online) The radial profile of toroidal rotation frequencies normalized by the Alfvén frequency at the plasma center. The bulk thermal ion rotation (solid) is compared with the electron rotation (dashed-dotted). The dashed vertical lines indicate the radial locations of rational surfaces with $q=m/n=2,3,4,5$, respectively.

sponse on the rotation model. At the rational surfaces, the electron flow model yields a larger response for the $m=2,3$ harmonics, but smaller response for the $m=4,5$ harmonics, compared to the ion flow model. This is essentially due to the fact that the electron flow, by amplitude, is slower than the ion flow at the $m=2,3$ rational surfaces, and faster at the $m=4,5$ rational surfaces (Fig. 25). In particular, the $m=3$ total response, with the electron flow, exceeds the external RMP field.

Figure 27 compares the radial field spectra, in terms of the peak amplitude along the plasma minor radius for all poloidal harmonics, between the external field, the total response field assuming the ion and the electron flow models, respectively. The $m<0$ nonresonant harmonics are not sensitive to the flow model used in the Ohm's law. The peak amplitude of resonant harmonics is generally not sensitive to the flow model either, except for the $m=3$ harmonic that corresponds to a nearly vanishing electron flow speed at the rational surface. This amplification for $m=3$ is also shown in the previous figure. The peak amplitude of $m>5$ nonresonant harmonics, interestingly, is also modified by the electron flow.

V. CONCLUSION AND DISCUSSION

We have presented a systematic study of various plasma parameters and coil configurations on the plasma response to the nonaxisymmetric fields produced by the RMP coils, based on MARS-F full toroidal computations. For this work,

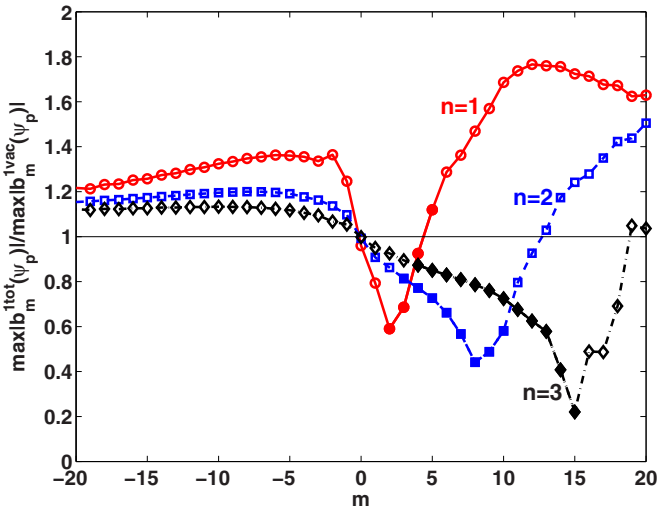

FIG. 24. (Color online) Ratio of the peak amplitude of total response field to that of the external field with different toroidal mode numbers n. The peak amplitude is defined as the maximal value of $b^1_m(\psi_p)$ over the plasma minor radius $0\le\psi_p\le1$. The resonant (nonresonant) harmonics are denoted by full (open) symbols.

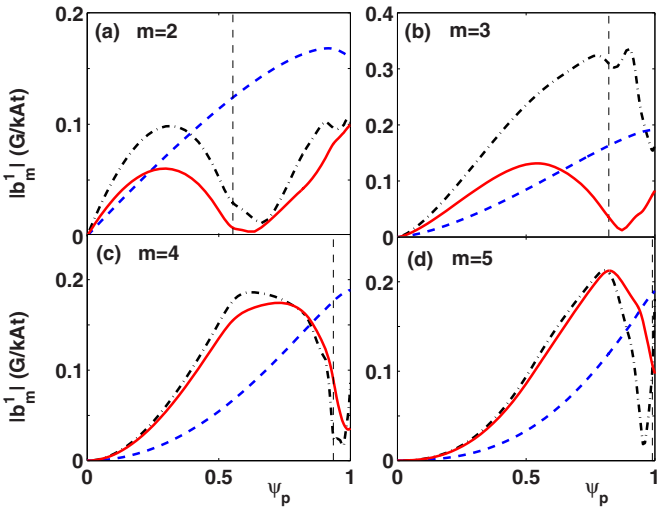

FIG. 26. (Color online) Comparison of radial profiles of the radial field component with ion flow (solid) against the electron flow (dashed-dotted) assumed in the Ohm's law for the resonant harmonics (a) $m/n=2/1$ and (b) $m/n=3/1$, (c) $m/n=4/1$ and (d) $m/n=5/1$. Plotted is also the external field (dashed lines) component produced by the RMP coils. The dashed vertical lines indicate the corresponding rational surfaces.

Downloaded 04 Apr 2012 to 129.16.35.96. Redistribution subject to AIP license or copyright; see http://pop.aip.org/about/rights_and_permissions

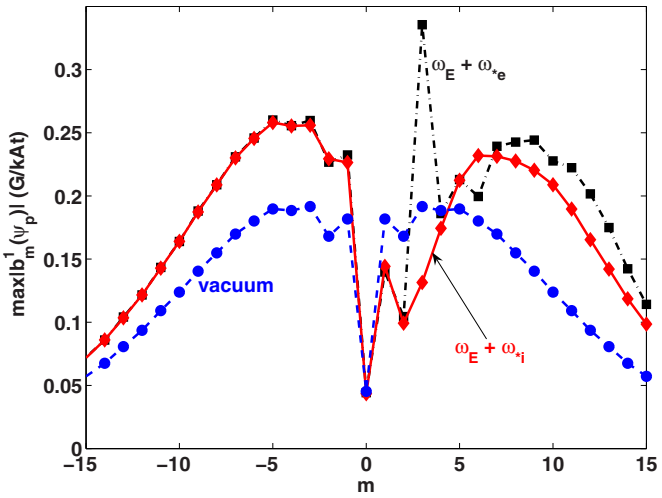

FIG. 27. (Color online) Comparison of the field spectra between the external field (dashed line), the total field assuming bulk ion flow (solid), and the total field assuming electron flow (dashed-dotted) in the Ohm's law. Shown is the peak amplitude (along the minor radius) of the poloidal Fourier harmonics of the $n=1$ radial magnetic field b^1. All harmonics are nonresonant except $m=2,3,4,5$.

we focused only on the magnetic field response of the plasma. A generic conclusion is that the plasma response does modify the external field for both resonant and nonresonant components. In particular, computations show that the $m<0$ nonresonant harmonics are always amplified by the plasma response (with convention that the resonant harmonics have $m>0$). The last point is also analytically demonstrated recently based on the MHD energy principle.[20]

The key plasma parameters affecting the RMP response are the plasma resistivity and rotation. The numerical results recover the analytic scaling laws versus the plasma resistivity and rotation frequency, in the asymptotic limits of large Lundquist number and fast rotation. While the ideal plasma response results in vanishing total field at rational surfaces (for resonant harmonics), the resistive response does allow a finite total field, hence the existence of magnetic islands. But the resistive plasma induced islands are normally much smaller than the vacuum islands. The toroidal plasma rotation can provide a strong shielding of the RMP field. At slow enough rotation, however, the plasma response can actually "amplify" the external field at rational surfaces.

Increasing the plasma pressure generally enhances the plasma response for both resonant and nonresonant harmonics. The plasma response experiences a qualitative change as the pressure approaches the no-wall limit for the ideal kink mode, as expected. The amplification of the $m<0$ nonresonant harmonics is sensitive to the plasma pressure. In fact, this appears to be the only sensitive plasma parameter that affects the $m<0$ nonresonant response.

Both midplane and off midplane odd parity coils trigger a (pure) plasma response with a similar poloidal mode structure, i.e., a similar plasma response. But the response amplitude can be several times larger with the internal coils, largely due to the coil proximity to the plasma surface. The off midplane coils with even parity trigger different plasma responses. The plasma response to the RMP coils, with different n numbers, is qualitatively similar.

Finally, a crude model, accounting for the electron diamagnetic flow effect, seems to suggest that the electron flow can play a significant role in the plasma response, in both the pedestal region and beyond (toward the plasma core). The fast electron flow in the pedestal region, due to large density (and temperature) gradient, reduces the response of resonant harmonics (i.e., screens the RMP field). But a stationary point of electron flow along the plasma minor radius (vanishing rotation speed, normally beyond the pedestal toward the inner plasma) tends to enhance the plasma response, compared to the ion flow model.

This work only aims at a systematic investigation of the resistive plasma response to the RMP fields. The results present one step forward, compared to the vacuum field theory, or the ideal response theory without plasma flow, in understanding the ELM mitigation physics. However, it is still questionable to apply these results directly to the ELM mitigation experiments due to the following limitations:

- We assumed a linear model for the plasma response to the RMP field. The key approximation here was that we fixed the plasma rotation while computing the field response. The true dynamics of the RMP field penetration is a nonlinear process, involving the coupling between the rotational screening of the RMP field and the rotational damping due to the RMP field. The latter effect will be studied in a future work.
- Our model is basically a single-fluid model, which is probably a reasonable model for describing the plasma core response. However, the sharp variation of the plasma equilibrium profiles, in the narrow pedestal region near the plasma edge, may require a more sophisticated model. We are currently working on a two-fluid version of MARS-F.
- The resistive-inertial layer response, adopted in MARS-F, is also an approximation. It is well known that the tearing layer, in the limit of narrow layer width, should involve at least a drift-kinetic description.
- Finally, experimental evidence seems to suggest an important role played by the plasma separatrix and the X-points for the ELM mitigation. The MARS-F model cannot deal with the exact X-point geometry.

ACKNOWLEDGMENTS

This work was funded by the RCUK Energy Programme under Grant No. EP/I501045 and the European Communities under the contract of Association between EURATOM and CCFE. The views and opinions expressed herein do not necessarily reflect those of the European Commission.

Y.Q.L. is grateful to Dr. M. S. Chu, Dr. R. J. Hastie, Dr. T. C. Hender, and Dr. F. L. Waelbroeck for many useful discussions. We also thank the anonymous reviewer for suggesting a study of the internal even parity coils.

[1]T. E. Evans, R. A. Moyer, K. H. Burrell, M. E. Fenstermacher, I. Joseph, A. W. Leonard, T. H. Osborne, G. D. Porter, M. J. Schaffer, P. B. Snyder, P. R. Thomas, J. G. Watkins, and W. P. West, Nat. Phys. **2**, 419 (2006).
[2]Y. Liang, H. R. Koslowski, P. R. Thomas, E. Nardon, B. Alper, P. Andrew,

Downloaded 04 Apr 2012 to 129.16.35.96. Redistribution subject to AIP license or copyright; see http://pop.aip.org/about/rights_and_permissions

Y. Andrew, G. Arnoux, Y. Baranov, M. Bcoulet, M. Beurskens, T. Biewer, M. Bigi, K. Crombe, E. De La Luna, P. de Vries, W. Fundamenski, S. Gerasimov, C. Giroud, M. P. Gryaznevich, N. Hawkes, S. Hotchin, D. Howell, S. Jachmich, V. Kiptily, L. Moreira, V. Parail, S. D. Pinches, E. Rachlew, and O. Zimmermann, Phys. Rev. Lett. **98**, 265004 (2007).
[3]A. Kirk, T. O'Gorman, S. Saarelma, R. Scannell, H. R. Wilson, and MAST Team, Plasma Phys. Controlled Fusion **51**, 065016 (2009).
[4]H. Reimerdes, J. Bialek, M. S. Chance, M. S. Chu, A. M. Garofalo, P. Gohil, Y. In, G. L. Jackson, R. J. Jayakumar, T. H. Jensen, J. S. Kim, R. J. La Haye, Y. Q. Liu, J. E. Menard, G. A. Navratil, M. Okabayashi, J. T. Scoville, E. J. Strait, D. D. Szymanski, and H. Takahashi, Nucl. Fusion **45**, 368 (2005).
[5]M. P. Gryaznevich, T. C. Hender, D. F. Howell, C. D. Challis, H. R. Koslowski, S. Gerasimov, E. Joffrin, Y. Q. Liu, S. Saarelma, and JET-EFDA Contributors, Plasma Phys. Controlled Fusion **50**, 124030 (2008).
[6]E. Nardon, M. Bécoulet, G. Huysmans, and O. Czarny, Phys. Plasmas **14**, 092501 (2007).
[7]M. Bécoulet, G. Huysmans, X. Garbet, E. Nardon, D. Howell, A. Garofalo, M. Schaffer, T. Evans, K. Shaing, A. Cole, J.-K. Park, and P. Cahyna, Nucl. Fusion **49**, 085011 (2009).
[8]D. Reiser and D. Chandra, Phys. Plasmas **16**, 042317 (2009).
[9]Q. Yu, S. Guenter, and K. H. Finken, Phys. Plasmas **16**, 042301 (2009).
[10]E. Nardon, P. Tamain, M. Bécoulet, G. Huysmans, and F. L. Waelbroeck, Nucl. Fusion **50**, 034002 (2010).
[11]M. F. Heyn, I. B. Ivanov, S. V. Kasilov, W. Kernbichler, I. Joseph, R. A. Moyer, and A. M. Runov, Nucl. Fusion **48**, 024005 (2008).
[12]V. A. Izzo and I. Joseph, Nucl. Fusion **48**, 115004 (2008).
[13]H. R. Strauss, L. Sugiyama, G. Y. Park, C. S. Chang, S. Ku, and I. Joseph, Nucl. Fusion **49**, 055025 (2009).
[14]F. L. Waelbroeck, Phys. Plasmas **10**, 4040 (2003).
[15]Y. Q. Liu, A. Bondeson, C. M. Fransson, B. Lennartson, and C. Breitholtz, Phys. Plasmas **7**, 3681 (2000).
[16]A. Bondeson and R. Iacono, Phys. Fluids B **1**, 1431 (1989).
[17]Y. Q. Liu, B. D. Dudson, Y. Gribov, M. P. Gryaznevich, T. C. Hender, A. Kirk, E. Nardon, M. V. Umansky, H. R. Wilson, and X. Q. Xu, *Proceedings of the 23rd International Conference*, Daejeon, 2010 (IAEA, Vienna, 2010) [Fusion Energy **CN180**, THS/P5-10 (2010)].
[18]R. Fitzpatrick, Phys. Plasmas **5**, 3325 (1998).
[19]Y. Q. Liu, I. T. Chapman, S. Saarelma, M. P. Gryaznevich, T. C. Hender, D. F. Howell, and JET-EFDA Contributors, Plasma Phys. Controlled Fusion **51**, 115005 (2009).
[20]M. S. Chu, L. L. Lao, M. J. Schaffer, T. Evans, E. J. Strait, Y. Q. Liu, M. J. Lanctot, H. Reimerdes, Y. Liu, T. Casper, and Y. Gribov, *Proceedings of the 23rd International Conference*, Daejeon, 2010 (IAEA, Vienna, 2010) [Fusion Energy **CN180**, THS/P5-04 (2010)].
[21]Y. Q. Liu, S. Saarelma, M. P. Gryaznevich, T. C. Hender, D. F. Howell, and JET-EFDA Contributors, Plasma Phys. Controlled Fusion **52**, 045011 (2010).
[22]M. J. Lanctot, H. Reimerdes, A. M. Garofalo, M. S. Chu, Y. Q. Liu, E. J. Strait, G. L. Jackson, R. J. La Haye, M. Okabayashi, T. H. Osborne, and M. J. Schaffer, Phys. Plasmas **17**, 030701 (2010).
[23]K. H. Burrell, T. E. Evans, E. J. Doyle, M. E. Fenstermacher, R. J. Groebner, A. W. Leonard, R. A. Moyer, T. H. Osborne, M. J. Schaffer, P. B. Snyder, P. R. Thomas, W. P. West, J. A. Boedo, A. M. Garofalo, P. Gohil, G. L. Jackson, R. J. La Haye, C. J. Lasnier, H. Reimerdes, T. L. Rhodes, J. T. Scoville, W. M. Solomon, D. M. Thomas, G. Wang, J. G. Watkins, and L. Zeng, Plasma Phys. Controlled Fusion **47**, B37 (2005).
[24]H. Reimerdes, A. M. Garofalo, E. J. Strait, R. J. Buttery, M. S. Chu, G. L. Jackson, R. J. La Haye, M. J. Lanctot, Y. Q. Liu, J.-K. Park, M. Okabayashi, M. Schaffer, and W. Solomon, Nucl. Fusion **49**, 115001 (2009).
[25]R. J. Hastie (private communication, 2010).
[26]J. W. Connor and R. J. Hastie, Plasma Phys. Controlled Fusion **27**, 621 (1985).

Downloaded 04 Apr 2012 to 129.16.35.96. Redistribution subject to AIP license or copyright; see http://pop.aip.org/about/rights_and_permissions